Cerea

Centre d'Enseignement et de Recherche en Environnement Atmosphérique

Habilitation à Diriger des Recherches

Université Paris-Est

Présentée et soutenue publiquement le 5 avril 2013 par

Karine Sartelet

Spécialité: Sciences et techniques de l'environnement

Modélisation de la qualité de l'air à l'échelle régionale

Jury composé de

P^{r} Hiroshi Hayami	CRIEPI	rapporteur
D^{r} Céline Mari	LA	rapporteure
P^{r} Robert Rossert	Université P. Sabatier	rapporteur
D^{r} Matthias Beekmann	LISA	examinateur
D^{r} Solène Turquety	LMD	examinatrice
P^{r} Christian Seigneur	CEREA	directeur d'habilitation

Préface

Ce mémoire présente mes travaux de recherche sur la modélisation de la qualité de l'air et des aérosols. Les améliorations des modèles de la qualité de l'air sont pertinentes pour obtenir de meilleures prévisions de la qualité de l'air et pour aider à la mise en place de politiques publiques efficaces. Mes travaux sur la qualité de l'air ont commencé en 2002 lors d'un premier post-doctorat au Pôle Air du Centre d'Enseignement et de Recherche sur l'Eau, la Ville et l'Environnement (CEREVE) sur la modélisation des concentrations en ozone autour de Paris, et le développement d'un modèle boîte pour représenter la dynamique des aérosols (approche modale, modèle MAM). Ils se sont ensuite poursuivis avec un post-doctorat au CRIEPI (Centre de recherche de l'industrie électrique du Japon) durant lequel j'ai finalisé le développement du modèle MAM, et je l'ai couplé au modèle de chimie transport Polair3D pour modéliser la qualité de l'air à Tokyo. J'ai ensuite mis en place une collaboration CEREA-CRIEPI pour le projet MICS Asie (inter-comparaison de modèles de qualité de l'air sur l'Asie) durant lequel j'ai comparé les simulations du modèle Polair3D sur l'Asie aux résultats d'autres modèles. A la fin de l'année 2005, j'ai commencé un post-doctorat au CEREA sur la modélisation des aérosols à l'échelle européenne et la compréhension des processus qui dominent la formation des aérosols. J'ai été embauchée en tant que chargée de recherche au CEREA à la fin de l'année 2007. Mes actions de recherche concernent l'amélioration des modèles numériques pour simuler la qualité de l'air, en combinant : (1) une meilleure représentation des processus physico-chimiques, (2) la confrontation du modèle aux données expérimentales, (3) l'identification des processus les plus incertains pour la formation des aérosols. J'ai encadré une post-doctorante, Elsa Real, sur la modélisation de l'impact des aérosols sur les taux de photolyse des gaz et sur les concentrations d'aérosols. J'ai travaillé avec le doctorant, Bastien Albriet, sur la modélisation des particules ultra-fines en sortie de pot d'échappement (couplage du modèle MAM à un modèle de mécanique des fluides). J'ai ensuite participé à l'encadrement d'un doctorant, Youngseob Kim, sur l'implémentation de schémas chimiques gazeux dans la plate-forme de la qualité de l'air Polyphemus et l'impact des différents schémas sur les concentrations de polluants (gaz et aérosols), ainsi que sur la modélisation météorologique à l'échelle urbaine. J'ai participé à une inter-comparaison de modèles de qualité de l'air sur l'Europe et l'Amérique du Nord dans le cadre du projet AQMEII (Air Quality Modelling Evaluation International Initiative), ainsi qu'à l'encadrement de deux doctorants sur la modélisation des aérosols (Florian Couvidat sur la modélisation des aérosols organiques et Hilel Dergaoui sur la modélisation du mélange des particules), et un doctorant sur l'assimilation de données lidar (Yiguo Wang). J'ai également travaillé avec Philippe Royer, étudiant en thèse de Patrick Chazette au Commissariat à l'énergie atomique, sur la comparaison de simulations de Polyphemus avec des données lidar sur Paris. J'encadre une doctorante, Stéphanie Deschamps, depuis l'automne 2011 sur la modélisation de la concentration en nombre des aérosols ; et un doctorant, Shupeng Zhu, depuis l'automne 2012 sur la modélisation du mélange des particules dans l'atmosphère. Je co-encadre égale-

ment depuis l'automne 2012 un doctorant, Charbel Abdallah, sur la modélisation des aérosols à Beyrouth (Liban).

Pour synthétiser mes différents travaux, j'ai choisi de les présenter selon 3 axes. Le premier axe concerne la modélisation "boîte" qui concerne la représentation des processus physico-chimiques qui influencent les concentrations d'aérosols dans un volume fixe homogène. Le deuxième axe concerne la comparaison des modèles aux observations et l'inter-comparaison de modèles de qualité de l'air. Le troisième axe concerne l'identification des processus les plus incertains dans la modélisation. Le dernier chapître du mémoire détaille les perspectives pour ces recherches.

Remerciements

Je tiens tout d'abord à remercier les membres de mon jury pour l'intérêt qu'ils ont porté à mes travaux, et pour s'être déplacés parfois de loin.

Je remercie Bruno Sportisse de m'avoir embauchée en tant que post-doctorat en 2002 puis en tant que chargée de recherche en 2007. Je le remercie également de m'avoir constamment soutenue dans mes projets de collaboration avec le CRIEPI.

Je souhaite adresser un merci particulier à Christian Seigneur pour ses nombreux conseils scientifiques qui ont permis à de nombreuses études d'aboutir à des résultats intéressants, ainsi que pour ses conseils en terme d'organisation et pour son soutien continuel.

Je souhaite également remercier Hiroshi Hayami de m'avoir accueillie au CRIEPI et de m'avoir permis de participer au projet MICS-Asie.

Un grand merci également aux différentes personnes avec qui j'ai eu la chance de travailler ces dix dernières années et qui ont grandement contribué au travail présenté ici : Florian Couvidat, Edouard Debry et Youngseob Kim sur la modélisation aérosols et multiphases, Yelva Roustan, Vivien Mallet, Denis Quélo et Jaouad Boutahar sur la modélisation avec Polair3D et Polyphemus, Patrick Chazette et Philippe Royer sur les comparaisons aux données lidar, Elsa Real sur les taux de photolyse, Marion Devilliers sur les particules ultrafines, Hilel Dergaoui sur le mélange externe, Victor Winiarek et Youngseob Kim sur WRF, Bastien Albriet, Kathleen Fahey et Marilyne Tombette pour leurs travaux sur les aérosols.

Un grand merci à Marc Bocquet et Yiguo Wang pour nos travaux sur l'assimilation de données lidar, à Bertrand Carissimo et Raphaël Bresson sur la modélisation aérosols à l'échelle locale,à Yang Zhang sur la comparaison Polyphemus/WRF-Chem.

Merci également aux différentes personnes non citées plus haut et qui travaillent dur en ce moment pour améliorer la modélisation des particules : Stéphanie Deschamps sur le nombre de particules, Shupeng Zhu sur le mélange externe, Charbel Abdallah sur la modélisation à Beyrouth et au Liban.

Un grand merci à Luc Musson Genon pour ses conseils, à Stéphanie Lacour pour les travaux et les moments partagés au CEREA.

Un grand merci à Sylvain Doré et Pierre Tran pour le support informatique ces dernières années et à Véronique Dehlinger pour son aide continuelle avec l'administration et les différentes missions.

Merci aux différentes personnes qui m'ont permis de participer aux projets AQMEII et MICS-Asie, et qui ont permis à l'ANR SAF-MED et au projet GMES-MDD d'être suffisamment aboutis pour être financés.

At last but not least, un grand merci à toute l'équipe passée et présente du CEREA pour sa bonne humeur et à Eve pour ses délicieux macarons !

Contents

1 Introduction **9**

2 Multiphase “box” models **13**
2.1 Gas phase . . . 13
2.2 Particle phase . . . 14
2.2.1 The modal and the sectional approaches . . . 14
2.2.2 Coagulation . . . 15
2.2.3 Nucleation . . . 17
2.2.4 Condensation/evaporation . . . 17
2.2.5 Numerical difficulties linked to modal distributions . . . 23
2.3 Cloud droplets . . . 25
2.4 Interaction between the gas and particle phases . . . 25
2.4.1 Heterogeneous reactions . . . 25
2.4.2 Impact of particles on photolysis rates . . . 25
2.5 Internal and external mixing . . . 26

3 Comparison of models to data and model inter-comparisons **31**
3.1 Model configurations . . . 31
3.1.1 Aqueous chemistry . . . 32
3.1.2 Land use cover . . . 32
3.1.3 Photolysis rates . . . 32
3.1.4 Dry and wet deposition . . . 32
3.1.5 Meteorology: vertical diffusion . . . 33
3.2 Model settings . . . 33
3.2.1 Over Europe . . . 33
3.2.2 Over North America . . . 34
3.2.3 Over East Asia . . . 35
3.2.4 Over Greater Paris . . . 35
3.2.5 Over Greater Tokyo . . . 35
3.3 Comparison to surface data . . . 39
3.4 Comparison to lidar data . . . 43
3.5 Model inter-comparisons . . . 45
3.5.1 Over East Asia: MICS . . . 47
3.5.2 Over Europe and North America: AQMEII . . . 50

4 Processes and uncertainties **55**
4.1 Conclusions from model inter-comparisons 55
4.2 Origins of uncertainties 56
4.3 Model intra-comparisons 58
4.3.1 Ozone 59
4.3.2 PM_{coarse} 59
4.3.3 $PM_{2.5}$ 60
4.3.4 Sulfate 61
4.3.5 Nitrate 61
4.3.6 Ammonium 61
4.3.7 Organic matter 62
4.4 Discussion 63

5 Perspectives **65**
5.1 Mixing properties of aerosols 65
5.2 Secondary Organic Aerosols 66
5.2.1 Chemical gas-phase mechanisms 66
5.2.2 Multiphase models 67
5.3 Modelling number concentrations 67
5.4 Model evaluations 68
5.5 Primary emissions 68
5.5.1 Anthropogenic emissions 68
5.5.2 Natural emissions 69
5.5.3 Resuspension of road dust 70

Chapter 1

Introduction

With the impact of air pollution on health and vegetation being a great concern, air quality models (AQMs) are often used at a regional scale to predict air quality; that is, to compute the distribution of atmospheric gases, aqueous-phase species, and particulate matter (PM). Particles, especially fine particles, leas to adverse effects on human health [e.g. Pope *et al.*, 1995], and to visibility reduction. They also affect the manner in which radiation passes through the atmosphere [Haywood et Boucher, 2000] and represent an uncertain component of climate changes due to direct and indirect effects on the Earth's radiative budget. The first motivation for better understanding the behaviour of atmospheric aerosols is then related to air quality, while the second one is related to climate change.

PM is a complex mixture of mineral dust, elemental carbon (EC) also referred to as black carbon or ligh-absorbing carbon, which may also contains some organic carbon, inorganic (sodium Na^+, sulfate SO_4^{2-}, ammonium NH_4^+, nitrate NO_3^-, chloride Cl^-) and organic (primary organic aerosol POA and surrogates of secondary organic aerosol SOA) components, with composition varying over the size range of a few nanometers to several micrometers. These particles can be emitted directly from various sources (e.g. natural such as biomass burning, sea-salt, dust, and anthropogenic) or can be formed in the atmosphere from the transformations of organic or inorganic precursor gases. Over Europe, annual-average $PM_{2.5}$ (particles of aerodynamic diameter lower than 2.5 μm) concentrations are primarily composed of carbonaceous compounds (EC and organic matter OM), nitrate, sulfate, and ammonium. Pio *et al.* [2007] reported similar concentrations of inorganic and organic compounds at non-urban locations. According to Airparif ("Origin of the particles in Île-de-France", September 2011, http://www.airparif.asso.fr/_pdf/publications/rapport-particules-110914.pdf), over Île-de-France, carbonaceous compounds represent from 40 to 65% of the total mass of annual average $PM_{2.5}$ concentrations, and inorganic species from 25 to 45%.

In Europe, concentrations of $PM_{2.5}$ and PM_{10} are regulated. $PM_{2.5}$ and PM_{10} annual concentrations should not exceed 25 and 40 μg m^{-3} respectively, and the daily PM_{10} concentrations should not exceed 50 μg m^{-3} more than 35 days per year. These regulatory thresholds for particles are frequently exceeded in Europe. According to seasons and places, the exceedances are due to inorganic compounds such as ammonium nitrate, organic compounds, desert dust or biomass burning, and more rarely to volcanic emissions. AQMs are powerful tools to assess the effects of proposed emission reductions on concentrations, and to evaluate whether the proposed emission reductions may help in attaining the regulatory thresholds, e.g. for ozone, nitrogen dioxide, PM_{10} and $PM_{2.5}$.

AQMs are composed of a series of modules that represent the physical and chemical processes that govern the concentrations of pollutants. Due to limitations in our understanding and computational resources, many processes are necessarily simplified or parameterised. Dispersion corresponds to transport by winds and mixing caused by turbulence. In AQMs, meteorological fields are often computed off-line, i.e. using a meteorological model, and the effects of particles on meteorology is thereby neglected. Chemical processes include gas-phase, aqueous-phase and particulate-phase chemical mechanisms, as well as the modelling of the dynamic evolution of the size distribution of particles and the interactions between the different phases, such as the heterogeneous reactions of gas-phase species at the particle surface. Deposition processes remove pollutants from the atmosphere and transfer them to other media.

The gas-phase chemical mechanism is an important component of AQMs, because secondary pollutants such as ozone and semi-volatile species (i.e. potential PM precursors) are formed during the gas-phase degradation of anthropogenic and biogenic compounds [e.g. Finlayson-Pitts et Pit 2000]. A mechanism that treats oxidant formation explicitly would require several millions of organic reactants and products and even more reactions [Aumont *et al.*, 2005]. Hence the chemical mechanisms used in three-dimensional AQMs must strike a balance between the complexity of the mechanism and its computational efficiency [Dodge, 2000]. Condensing a chemical kinetic mechanism to minimise computational requirements necessarily introduces approximations that are reflected as uncertainties in the mechanism simulations.

Particles are often assumed to be internally mixed, that is particles of a given size are associated to a unique chemical composition. On the opposite, under the external mixing assumption, particles of a given size can have different chemical compositions. Although the PM size distribution may be modelled by different approaches, in AQMs, it is often modelled using the sectional distribution [e.g. Debry *et al.*, 2007] or the modal distribution [e.g. Sartelet *et al.*, 2006]. PM "box" models usually take into account the processes of coagulation (collision of particles due mostly to their Brownian motion), condensation/evaporation (mass transfer between gas and PM phases) and nucleation (formation of PM from the gas phase). The PM composition and mass distribution are strongly influenced by condensation/evaporation processes. Two approaches may be used to model these processes: a dynamic approach (mass transfer is explicitly taken into account) or an equilibrium approach (thermodynamic equilibrium is assumed between the gas and PM phases). Although this assumption may be valid for small particles (diameters < 1 μm), it may not hold for larger particles. However, it is often used for all particle sizes, because it is computationally fast.

Organic aerosols (OA) are a significant fraction of PM. Concentrations of organic aerosols are important in winter because of combustion emissions and the presence of semi-volatile organic aerosols, while in summer the concentrations of organic aerosols are mainly due to biogenic compounds. They are often dominated by secondary organic aerosol (SOA), formed from the condensation of low-volatility oxidised gas-phase organic compounds. Although the formation of inorganic matter is relatively well understood, the modelling of OM, which involves a large number of existing organic species and complex chemical reactions/condensation pathways, is more difficult. At the global and European scales, it is usually considered that the biogenic fraction largely dominates the SOA budget. Biogenic emissions are mostly made of volatile organic compounds VOC (e.g. isoprene, terpenes), that may be oxidised and then condense onto particles or form new particles. Because the oxidation of biogenic VOC is enhanced by anthropogenic plumes, reducing anthropogenic emissions may actually reduce the biogenic OA concentration.

These examples of key aspects of air quality modelling highlight the need to develop models (mechanisms and parameterisations) that are both realistic and computationally efficient. The following sections describe the development of such models and their evaluations.

Chapter 2

Multiphase “box” models

“Box” models refer to mathematical representation of physical and/or chemical processes in a fixed volume of uniform properties (pressure, temperature, concentrations, etc.). They can be used to describe the atmospheric multiphase mixture of gas-phase species, particles and cloud droplets.

2.1 Gas phase

Secondary pollutants such as ozone (O_3) and PM precursors are formed during the gas-phase degradation of anthropogenic and biogenic compounds: oxides of nitrogen (NO_x, the sum of NO and NO_2) and volatile organic compounds (VOCs). In the boundary layer, a key oxidant is the hydroxyl (OH) radical, because of its relatively high concentration and because it reacts with most trace species. Because of its health impact and its link to the oxidation capacity of the atmosphere, the formation and destruction of O_3 have been extensively studied. O_3 is influenced by photochemistry, e.g. the photodissociation of O_3 leads to the production of OH radicals, while the photodissociation of NO_2 leads to the production of O_3, as well as by the relative importance of NO_x and VOCs. Because of the importance of photochemistry, daytime chemistry and nighttime chemistry differ, e.g. nitrate (NO_3) radicals become dominant at night.

A mechanism that treats oxidant formation explicitly would require several millions of organic reactants and products and even more reactions [Aumont *et al.*, 2005]. Hence the chemical mechanisms used in three-dimensional AQMs must strike a balance between the complexity of the mechanism and its computational efficiency. Condensing a chemical kinetic mechanism to minimise computational requirements necessarily introduces approximations that are reflected as uncertainties in the mechanism simulations.

Condensed chemical mechanisms for tropospheric ozone formation are mostly classified as lumped structure mechanisms and lumped species mechanisms. In a lumped structure mechanism, chemical organic compounds are divided into smaller species elements (functional groups) based on the types of carbon bonds in each species. In a lumped species mechanism, a particular organic compound or a surrogate species is used to represent several organic compounds of a same class (e.g., alkanes, alkenes and aromatics) which, for example, have similar reactivity with hydroxy radicals. In the lumped structure category, commonly used mechanisms are CB05 [Yarwood *et al.*, 2005] and its predecessors. In the lumped species category, commonly used mechanisms are RACM [Stockwell *et al.*, 1997], RACM2 [Goliff et Stockwell, 2008] or SAPRC [Carter, 2010] and their predecessors.

As organic gases are oxidised in the gas phase by OH, O_3 and NO_3, their volatility evolves. Their volatility may decrease by the addition of polar functional groups (such as hydroxyl, hydroperoxyl, nitrate and acid groups). On the other hand, oxidation products may have higher volatility than the parent organic gases due to the cleavage of carbon-carbon bonds. Products of low volatility may condense on the available particles to establish equilibrium between the gas and particle phases. The formation of these semi-volatile organic species (SVOC) is often not considered in the mechanisms described previously, which were originally developped to model O_3 concentrations. To link these mechanisms to organic aerosol models [e.g. Schell *et al.*, 2001; Couvidat *et al.*, 2012a], additional oxidation products corresponding to surrogate SVOC species are added to molecule-based chemical mechanisms. Additional molecule-based species also often needs to be added to carbon-bond mechanisms, such as CB5, in order to represent these oxidation products. Organic aerosol models often consider that SVOCs are formed after one oxidation step, whereas several oxidation steps may be required to correctly model SVOCs responsible for SOA formation [e.g. Lee-Taylor *et al.*, 2011].

Our work in gas-phase chemistry has focused on the coupling of gas-phase chemical kinetic mechanisms with aerosol modules, and the intercomparison of gas-phase mechanisms in terms of ozone (O_3) and secondary PM formation (see section 4.3).

2.2 Particle phase

The PM size distribution may be modelled by different approaches, among which the most common in AQMs are the sectional size distribution [the size distribution is discretised into sections or "bins", e.g., Debry *et al.*, 2007] and the modal size distribution [the size distribution is discretised into log-normal modes, e.g., Sartelet *et al.*, 2006]. Internal mixing is often assumed, i.e. a chemical composition is associated to each particle size range (to each bin or mode).

Our work in this area has focused on the development of improved numerical methods for the solution of the genral dynamic equation (GDE) using both the modal and the sectional approaches, and the development of a general approach to model externally mixed particles.

2.2.1 The modal and the sectional approaches

Let us denote $n(v,t)$ the number of aerosols, which volume ranges between v and $v+dv$. Particles are assumed to be spherical and the diameter d_p is often used instead of the volume v.

In sectional models, the aerosol distribution is described by a sum of sections. Let us denote n_s the number of sections. In each section i, the number $N_i(t)$ and the mass $Q_i(t)$ of particles are constant:

$$N_i(t) = \int_{d_i^-}^{d_i^+} n_i\left(d_p,t\right) dd_p \tag{2.1}$$

$$Q_i(t) = \int_{d_i^-}^{d_i^+} q_i\left(d_p,t\right) dd_p = \frac{\pi}{6}\rho_i \int_{d_i^-}^{d_i^+} d_p^3\, n_i\left(d_p,t\right) dd_p \tag{2.2}$$

where $q_i\left(d_p,t\right)$ is the mass concentration of particles of diameter d_p, ρ_i is the density of particles, and d_i^- and d_i^+ are the lower and upper bounds of the section i. The diameter $d_{p,i}$ of

particles in section i can be diagnosed using the relation

$$Q_i = \frac{\pi}{6}\, d_{p,i}^3\, N_i \tag{2.3}$$

In modal models, the aerosol distribution is described as a sum of log-normal modes $n_i(d_p, t)$

$$n_i(d_p) \;=\; \frac{N_i}{\sqrt{2\pi}\ln(\sigma_{g,i})} \exp\left[-\frac{1}{2}\frac{\ln^2(d_p/d_{g,i})}{\ln^2(\sigma_{g,i})}\right] \tag{2.4}$$

where N_i is the total number of aerosols in the mode i, $d_{g,i}$ is the median diameter, d_p is the particle diameter and $\sigma_{g,i}$ is the standard deviation of the mode. The mode distribution is known once the three parameters N_i, $d_{g,i}$ and $\sigma_{g,i}$ are. To derive the dynamical equations of the modal distribution, moments are used. The moment of order h of the distribution is defined as

$$M_{h,i} \;=\; \int_{-\infty}^{\infty} d_p^h\, n_i(d_p)\, d(d_p) \tag{2.5}$$

which leads to

$$M_{h,i} = N_i d_{g,i}^h \exp\left(\frac{h^2}{2}\ln^2\sigma_{g,i}\right). \tag{2.6}$$

The three parameters N_i, $d_{g,i}$ and $\sigma_{g,i}$ may be computed from the three moments $M_{0,i}$, $M_{3,i}$ and $M_{6,i}$ as follows:

$$N_i = M_{0,i} \tag{2.7}$$

$$d_{g,i} = \left(\frac{M_{3,i}^4}{M_{6,i}M_{0,i}^3}\right)^{\frac{1}{6}} \tag{2.8}$$

$$\sigma_{g,i} = \exp\left(\sqrt{\frac{1}{9}\ln\left(\frac{M_{0,i}M_{6,i}}{M_{3,i}^2}\right)}\right) \tag{2.9}$$

Note that the moments are related to physical quantities:

- $M_{0,i}$ is the total number N_i of aerosols
  $$M_{0,i} = N_i,$$
- $M_{3,i}$ is proportional to the total volume of aerosols per volume of air
  $$M_{3,i} = \tfrac{6}{\pi} V_i.$$

The PM distribution evolves under the effect of different processes. Those strongly related to the particle phase are coagulation, nucleation and condensation/evaporation.

2.2.2 Coagulation

Atmospheric particles may collide with one another due to their Brownian motion or due to other forces (e.g., Van der Walls: attractive and repulsive forces between molecules). Brownian coagulation is believed to be the dominant mechanism in the atmosphere.

By Brownian coagulation, the number distribution evolves as follows:

$$\left(\frac{\partial n}{\partial t}\right)_{coag} = \frac{1}{2}\int_0^v \beta(v', v-v')n(v)n(v-v')dv' - \int_0^\infty \beta(v,v')n(v)n(v')dv' \tag{2.10}$$

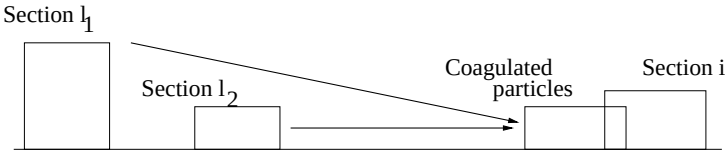

Figure 2.1: Coagulation between sections l_1 and l_2

where $\beta(v, v') = \beta(v', v)$ is the Brownian coagulation coefficient between particles of volume v and v'.

In the sectional approach, when particles coagulate, the resulting particles may belong to sections different from the initial section in which the particles were. Each section i is defined by fixed diameter bounds $d^-_{p,i}$ and $d^+_{p,i}$. As shown in Figure 2.1, when particles of two sections l_1 and l_2 coagulate, part of these coagulated particles belongs to the section i, i.e. their diameter belongs to $[d^-_{p,i}, d^+_{p,i}]$. This part is represented by a partition coefficient $R^i_{l_1 l_2}$. By defining partition coefficients, which redistribute coagulated sections into the initial sections, the evolution equation for the number concentration of a section i may be written as follows:

$$\frac{dN_i(t)}{dt} = \frac{1}{2}\sum_{l_1=1}^{i}\sum_{l_2=1}^{i} K_{l_1 l_2} R^i_{l_1 l_2} N_{l_1}(t) N_{l_2}(t) - N_i(t)\sum_{l=1}^{s_m} K_{il} N_l(t) \tag{2.11}$$

where s_m is the number of sections, the coagulation kernel coefficient $K_{l_1 l_2}$ is assumed constant over the sections
$[d^-_{p,l_1}, d^+_{p,l_1}]x[d^-_{p,l_2}, d^+_{p,l_2}]$. Following Jacobson *et al.* [1994] and as detailed by Debry et Sportisse [2007], the partition coefficient may be simplified as

$$R^i_{l_1 l_2} = \frac{1}{L_1 L_2}\int_{m^-_{l_2}}^{m^+_{l_2}}\int_{d^-_{p,l_1}}^{d^+_{p,l_1}} E^i(u, v)\, du\, dv \tag{2.12}$$

with L_1 the width of section l_1, $E^i(u, v)$ is equal to 1 if the formed particle is in section i, 0 otherwise.

Similarly, the evolution of the mass distribution in section i may be written as

$$\frac{dQ_i(t)}{dt} = \sum_{l_1=1}^{i}\sum_{l_2=1}^{i} K_{l_1 l_2} R^i_{l_1 l_2} Q_{l_1}(t) N_{l_2}(t) - Q_i(t)\sum_{l=1}^{n_s} K_{il} N_l(t) \tag{2.13}$$

With the modal approach, because of the log-normal shapes of the modes, it is more difficult to define partition coefficients. The evolution equation for each mode is obtained by substituting $n(d_p, t)$ by the sum of the log-normal modes (for example for 3 modes i, j and k, $n(d_p, t) = n_i(d_p, t) + n_j(d_p, t) + n_k(d_p, t)$) in equation (2.14) and by making the following hypotheses:

- When particles from the same mode collide (intra-modal coagulation), the agglomerated particle remains in that mode.

- When particles from two different modes collide (inter-modal coagulation) the agglomerated particle is assigned to the mode with the larger mean size.

The evolution equation of the moments of order h may be written as

$$\left(\frac{\partial M_h}{\partial t}\right)_{coag} = \frac{1}{2}\int_0^\infty \int_0^\infty \left(d_{p_1}^3 + d_{p_2}^3\right)^{h/3} \beta(d_{p_1}, d_{p_2}) n(d_{p_1})\ n(d_{p_2})\ d(d_{p_1}) d(d_{p_2}) - \frac{1}{2}\int_0^\infty \int_0^\infty \left(d_{p_1}^h + d_{p_2}^h\right) \beta(d_{p_1}, d_{p_2})\ n(d_{p_1}) n(d_{p_2})\ d(d_{p_1}) d(d_{p_2}) \quad (2.14)$$

Appendix 1 details the evolution equation of the moments with 3 modes.

2.2.3 Nucleation

The smallest particles are formed by the aggregation of gaseous molecules leading to thermodynamically stable clusters. The mechanism is poorly known and most nucleation parameterisations used in AQMs assume homogeneous binary nucleation of sulfate and water to be the major mechanism in the formation of new particles [e.g. Kuang *et al.*, 2008; Vehkamaki *et al.*, 2002, 2003]. Binary schemes tend to under-predict nucleation rates in comparison to observed values, and sulfuric acid-ammonia-water ternary nucleation parameterisations have been developed [e.g. Napari *et al.*, 2002]. Nucleation of organic molecules may also occur, particularly over forests in pristine areas [Went, 1960] and such nucleation processes have been tentatively reproduced in the laboratory [Boulon *et al.*, 2013]. However, the most relevant and complex nucleation processes may be the formation of ultrafine particles in car exhausts, which may involve both sulfuric acid and organic molecules [Albriet *et al.*, 2010; Seigneur, 2009].

In the sectional approach, the evolution equations of number and mass are

$$\left(\frac{\partial N_i}{\partial t}\right)_{nuc} = J \quad (2.15)$$

$$\left(\frac{\partial Q_i}{\partial t}\right)_{nuc} = J\ \rho_i \frac{\pi}{6} d_{g_0}^3 \quad (2.16)$$

where J is the nucleation rate, ρ_i the density of particles, d_{g_0} and σ_{g_0} are the mean diameter and the standard deviation of aerosols that nucleate. In the modal approach, the rate of change of moments due to nucleation may be written as

$$\left(\frac{\partial M_h}{\partial t}\right)_{nuc} = J d_{g_0}^h . \exp\left(\frac{k^2}{2} \ln^2 \sigma_{g_0}\right) \quad (2.17)$$

Uncertainties in the nucleation parameterisation schemes are quite large. Zhang *et al.* [2010] found differences by several orders of magnitude among the nucleation rates for sulfate particles calculated with 12 different parameterisations under the same meteorological and chemical conditions. Recent studies also derived empirical parameterisations to model nucleation as a function of atmospheric ion concentrations and low-volatile organic vapours [Nieminen *et al.*, 2011; Paasonen *et al.*, 2010]. Similarly to ammonia, amines may react with sulfuric acids in the atmosphere to participate to the nucleation of new particles [Erupe *et al.*, 2011].

2.2.4 Condensation/evaporation

Some gas-phase species with a low saturation vapour pressure may condense on existing particles while some species in the particle phase may evaporate. This mass transfer is governed

by the gradient between the gas-phase concentration and the concentration at the surface of the particle.

The condensation/evaporation term is

$$\left(\frac{\partial n}{\partial t}\right)_{cond} = -\frac{\partial\left(I_0 n\right)}{\partial m} \tag{2.18}$$

where $I_0(v,t) = \frac{\partial m}{\partial t}$ is the rate of change of the total mass of a particle of mass m as a result of condensation/evaporation processes (I_0 is positive in case of condensation and negative in case of evaporation) For a species s, it may be written as

$$I_{0,s}(d_p,t) = 2\pi D_s\ d_p^w\ f(Kn_i,\alpha_i)\left(c_s - c_s^{eq}\ \eta(d_p^w)\right), \tag{2.19}$$

with d_p^w the wet diameter of particles, c_s the concentration of species s in the gas phase, c_s^{eq} the aerosol surface concentration at equilibrium with the aerosol mixture, D_s the diffusivity of species s in air, $Kn_i = 2\ \lambda_s/d_p^w$ the Knudsen number, λ_s the mean free path of species s in air, $f(Kn_i,\alpha_i)$ a correction factor for non-continuum effects and imperfect accommodation [Dahneke, 1983], α_i an accommodation coefficient (between 0 and 1) and η the Kelvin effect correction coefficient. This coefficient models the effect of the curvature of small particles, which leads to an increase of the saturation vapor pressure of chemical compounds, making their condensation more difficult and favouring their evaporation.

For the sectional distribution, using a Lagrangian approach by letting the section bounds evolve, and assuming that the number of particles is uniformly constant between the bounds, the condensation/evaporation term may be written as [Debry et Sportisse, 2006]

$$\left(\frac{\partial N_i}{\partial t}\right)_{cond} = 0 \tag{2.20}$$

$$\left(\frac{\partial Q_{i,s}}{\partial t}\right)_{cond} = N_i\ I_{0,i,s}(d_{p,i}) \tag{2.21}$$

and for the modal distribution, it may be written as

$$\left(\frac{\partial M_h}{\partial t}\right)_{cond} = \frac{2h}{\pi\ \rho}\int_0^\infty d_p^{h-3} I_v\ n(d_p,t)\ d(d_p). \tag{2.22}$$

where $I_v(v,t) = \frac{\partial v}{\partial t}$ is the rate of change of the total volume of a particle of volume v as a result of condensation/evaporation processes. For a species s of density ρ_s, it may be written as

$$I_{v,s}(d_p,t) = \frac{I_{0,s}(d_p,t)}{\rho_s}. \tag{2.23}$$

To gain computational time, the concentration in the bulk gas phase is often assumed to be equal to that at the particle surface, i.e. to be at local thermodynamic equilibrium with the particle composition. In other words, the dynamic modelling may be replaced with an assumption of thermodynamic equilibrium between the bulk gas and PM phases. Although this assumption may be valid for small particles (diameters <1 μm), several measurements [e.g. Allen *et al.*, 1989], as well as studies of time scales required to reach thermodynamic equilibrium [e.g. Wexler et Seinfeld, 1990], have shown that the assumption of thermodynamic equilibrium may not hold for larger particles [e.g. Pilinis *et al.*, 2000]. Although the equilibrium approach is less accurate than the dynamic approach, it is attractive because it is computationally fast.

2.2.4.1 Redistribution or mode-merging schemes

For 3-D applications, the sections or modes need to be of distinct size ranges throughout the simulations. As particles grow/shrink with condensation/evaporation, the bounds of the sections or modes evolve, and it is necessary to redistribute the number and mass or moments, introducing numerical errors.

In the sectional approach, the section bounds are usually fixed. The number, the mass concentrations and the diameter of each section are linked through the equation (2.3). Redistribution occurs when the diameter of a section increases or decreases beyond the section boundaries. The key point in redistributing sections after condensation/evaporation is to choose which of the two variables amongst mass, number and diameter to conserve and which to diagnose. Different approaches exist depending on whether the mean diameter of the section is allowed to vary or not (Devilliers *et al.* [2013]).

In the modal approach, different mode merging schemes may be used, often based on that of Binkowski et Roselle [2003], where a threshold diameter between the two modes to be merged is chosen as the diameter where the number distributions of the two modes overlap. Mode merging may also be applied for each mode when the diameter of the distribution exceeds a fixed diameter (Sartelet *et al.* [2007b]).

2.2.4.2 Inorganic compounds

The inorganic compounds usually considered are sodium Na^+, sulfate SO_4^{2-}, ammonium NH_4^+, nitrate NO_3^- and chloride Cl^-, and sometimes crustal species (Ca^+, K^+, Mg^{2+}) which can affect thermodynamic equilibrium where dust concentrations are large. Sulfate formed from the nucleation or condensation of gaseous sulfuric acid (H_2SO_4) has a low saturation vapour pressure and easily condenses onto particles. In the particle phase, sulfate may be neutralised by ammonium, which is formed from the condensation of ammonia (NH_3). Ammonium may also be neutralised by nitrate formed from the condensation of nitric acid (HNO_3). Particles may be solid or in an aqueous solution. A solid particle transforms into an aqueous solution when the relative humidity reaches a specific level called the Mutual Deliquescence Relative Humidity (MDRH), which is a function of the composition of the particle. The aerosol water content is often approximated by the Zdanovskii-Stokes-Robinson (ZSR) relation, which states that the total aerosol water content at a particular relative humidity is the sum of the water content of each chemical component of the particle.

Departure from thermodynamic equilibrium drives the mass transfer of species between gas and particle phases. Thermodynamic models are used to compute the concentrations of gas and particles at equilibrium.

Some models, such as AIM2 [Wexler et Clegg, 2002], use a Gibbs free energy minimisation method to determine the thermodynamic equilibrium state. As this method is computationally expensive, other models rather solve a reduced set of equilibrium reactions. As the particle phase is concentrated, it is non ideal (intermolecular interactions between chemical compounds are strong) and the equilibrium constants of reactions depends on activity coefficients (EQUISOLVII Jacobson [1999], ISORROPIA Nenes *et al.* [1999]), leading the set of equilibrium equations to be highly nonlinear. To gain computational time, these coefficients may be tabulated depending on the composition (e.g. ISORROPIA), and/or only equations involving components which are in non-negligeable quantities are considered (e.g. ISORROPIA, SCAPE2 Meng *et al.* [1995]).

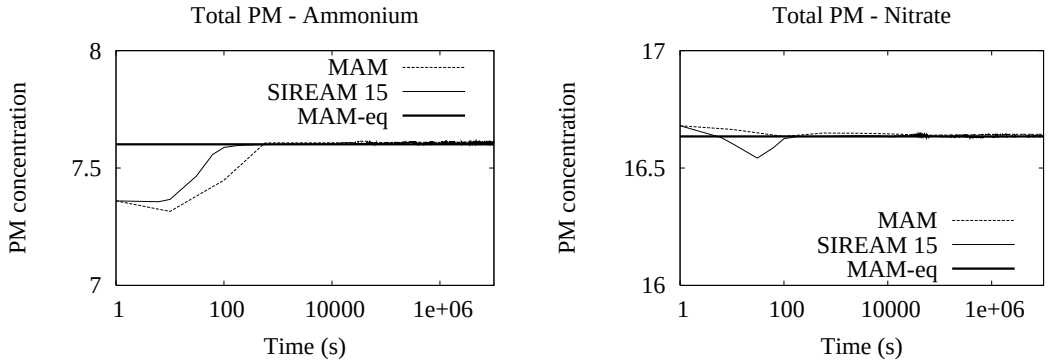

Figure 2.2: Time variation of ammonium and nitrate in μg m^{-3}), using measured gas and PM concentrations on 23 November 1999 at Komae as initial conditions [Sartelet *et al.*, 2006].

Most thermodynamic models compute the global equilibrium between gas and particle phases, i.e. from the total concentration of a component (e.g. ammonium in the particle phase and ammonia in the gas phase), it will determine the gas concentration (ammonia) and the particle concentration (ammonium). Others, such as ISORROPIA, may also solve the reverse problem and provide the surface concentrations of gases at equilibrium from the particle concentrations. These surface concentrations are the concentrations c_s^{eq} involved in the condensation/evaporation equation.

In case of liquid particles, for numerical stability, limiting the acidity flux proportionally to the particle hydrogen ion concentration leads to correction in the surface concentrations of PM, as done by Debry et Sportisse [2006] and Pilinis *et al.* [2000].

The evolutions of gaseous concentrations can be deduced from the evolution of particle-phase concentrations by mass conservation.

If global thermodynamic equilibrium is assumed, the partitioning between particle and gas phases is first computed using the thermodynamic model, and a weighting scheme is used to redistribute total particle equilibrium concentrations between the particles of different sizes (bins or sections). The weighting scheme may depend on the initial concentration of sulfate in each mode [Sartelet *et al.*, 2006; Binkowski et Roselle, 2003] or on the condensation/evaporation kernel of the condensation/evaporation rate [Sartelet *et al.*, 2006; Debry *et al.*, 2007]. The evolution equation of condensation/evaporation is then only used to compute the rate of species of low volatility such as sulfate.

Sartelet *et al.* [2006] compared the concentration of nitrate, ammonium and chloride obtained using a sectional model with 15 sections (SIREAM-15), a modal model (MAM) with 4 modes and a modal model assuming thermodynamic equilibrium (MAM-eq). Initial conditions and meteorological variables were obtained from daily-averaged measurements made on two highly polluted days, 23 November 1999 and 25 June 2001, in Komae (Japan). Differences between MAM and SIREAM are very low at equilibrium, although the time to reach equilibrium differs between the two models (see Figures 2.2 and 2.3). Assuming global thermodynamic equilibrium may also lead to significant difference in PM concentration, as shown in Figure 2.3.

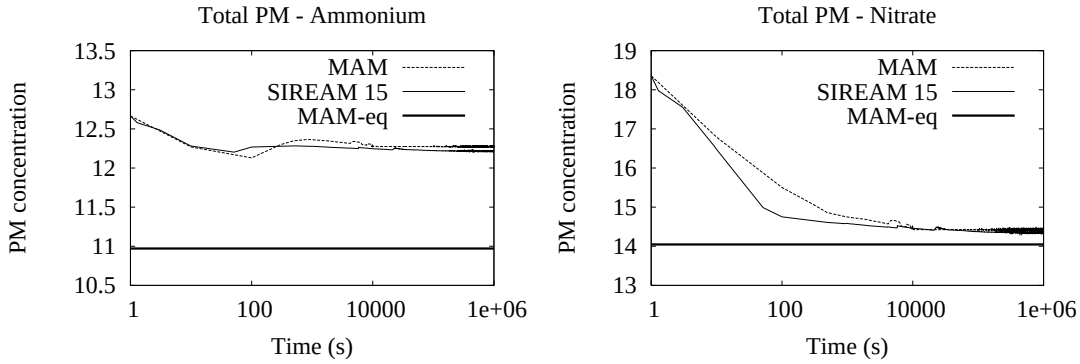

Figure 2.3: Time variation of ammonium and nitrate in μg m^{-3}), using measured gas and PM concentrations on 25 June 2001 at Komae as initial conditions [Sartelet *et al.*, 2006].

2.2.4.3 Secondary organic aerosols

The oxidation of VOCs leads to species (SVOCs) that have increasingly complicated chemical functions, high polarisations, and lower saturation vapour pressure. There are many uncertainties surrounding the formation of secondary organic aerosol. Due to the lack of knowledge and the sheer number and complexity of organic species, most chemical reaction schemes for organics are very crude representations of the true mechanism. These typically include the lumping of representative organic species and highly simplified reaction mechanisms.

SOA modelling has undergone significant progress over the past few years due to the rapid increase of experimental data on SOA yields and molecular chemical composition resulting from the oxidation of a variety of VOC and SVOC. SOA models can be grouped into two major categories: (1) models based on an empirical representation of SOA formation and (2) models based on a mechanistic representation of SOA formation. Models of the first category include the widely used two-compound Odum approach [Odum *et al.*, 1996] and the more recent volatility basis set (VBS) approach [Donahue *et al.*, 2006, 2011]. In the two-compound Odum approach, the oxidation of a VOC precursor is approximated by a reaction with 2 lumped products P_1 and P_2 which are semi-volatile and can condense onto the particle phase:

$$VOC + \text{Oxidant} \Rightarrow \alpha_1 P_1 + \alpha_2 P_2 \tag{2.24}$$

The stochiometric coefficients, as well as the partitioning constants between the gas and particle phases of each product are estimated from chamber experiments. Although the molecular structure of the products are usually unknown, the total organic particle mass and the partitioning between the gas and particle phases is obtained from the model of Pankow [Pankow, 1994] by resolving iteratively

$$M_0 = \sum_{i=1}^{n} C_{p,i} = \sum_{i=1}^{n} C_{tot,i} * \frac{K_{p,i}\, M_0}{1 + K_{p,i}\, M_0} \tag{2.25}$$

where n (=2) is the number of semi-volatile products, $C_{p,i}$ is the concentration in the particle phase of compound i, $C_{tot,i}$ is the sum of the concentrations in the gas and particle phases of

compound i and $K_{p,i}$ the partitioning constant

$$K_{p,i} = \frac{C_{p,i}}{C_{g,i}} \frac{1}{M_0} = \frac{1}{C_i^*} \tag{2.26}$$

with C_i^* the saturation concentration of i in the organic mixture. The partitiong constants vary with temperature as modelled by the Clausius-Clapeyron equation which relates it to δH^{vap} the difference between the enthalpy of the vapor and the liquid state. Effective values of δH^{vap} are determined empirically from the temperature transformation of bulk SOA. In the 1D (one dimensional) VBS approach, organic compounds are divided in logarithmically-spaced bins of similar saturation concentration C_i^*, i.e. of similar volatility, and the gas-particle partitioning is obtained from Equation (2.25). Oxidation moves organic compounds from one bin to the other. Epstein *et al.* [2010] derived a semi-empirical correlation between enthalpy of vaporization, temperature and saturation concentration of organic aerosols. In the 2D-VBS approach, organic compounds are described not only by C_i^*, but also by their oxygen content O:C, i.e. their oxidative state.

Models of the second category use experimental data (or theoretical mechanism data) on the molecular composition of SOA and represent the formation of SOA using surrogate molecules with representative physico-chemical properties for gas/particle partitioning [Couvidat *et al.*, 2012a]. Precursors of SOA in the models typically include anthropogenic compounds (aromatics, long-chain alkanes and long-chain alkenes) and biogenic compounds (isoprene, monoterpenes, and sesquiterpenes). The gas/particle partitioning includes both absorption into hydrophobic organic particles and dissolution into aqueous particles. Absorption of SOA into organic particles follows Raoult's law and depends on the average molecular weight of the organic particulate mixture, the saturation vapor pressure of the condensing SOA surrogate and its activity coefficient in the particle. Absorption of hydrophilic SOA into aqueous particles follows Henry's law and depends on the liquid water content of the particle, its pH and the activity coefficients of the dissolved species. The non-ideality of the mixture can be taken into account by the activity coefficient γ_i: $C_i^* = \gamma_i \, C_i^0$ with C_i^0 the saturation concentration over a pure liquid. Activity coefficients are computed by the universal functional activity coefficient (UNIFAC) method, which deduces the intermolecular interactions from the molecules' groups contribution.

A recent comparison of the Odum empirical approach and of the mechanistic model AEC highlighted which components of an SOA model are the most relevant (completeness of the precursor VOC list, ideal mixing assumption treatment of oligomerization, importance of low-NOx vs. high-NOx regimes, treatment of hydrophilic isoprene SOA) [Kim *et al.*, 2011a]. Oligomerization is the process by which several monomers combine themselves into a heavier component, thus reducing the monomer concentration and favouring its further condensation. In the mechanistic approach, it can be represented according to a pH dependent parameterization [Pun et Seigneur, 2007] for glyoxal and methyl-glyoxal. Because most SOA formation at the regional scale occurs under low-NOx conditions, SOA yields increase when one allows the mechanism to treat both high- and low-NOx regimes. The effect depends, however, on how the low- NOx versus high-NOx regimes are implemented in the gas phase chemical kinetic mechanism. SOA formed from isoprene oxidation are believed to be hydrophilic and, therefore, may absorb into aqueous particles rather than into hydrophobic organic particles. The affinity of those SOA compounds for aqueous particles is significantly larger than for organic particles, which could lead to greater SOA formation under humid conditions [Couvidat et Seigneur,

2011].

Although the empirical and mechanistic models are fundamentally different in their initial design, they aim at describing the same processes. Furthermore, they will tend to converge as they continue to be developed and refined. For example, the VBS scheme can take into account the oxidative state of SOA [Donahue *et al.*, 2011, 2D-VBS] and approximations of activity coefficients can be used in the 2D-VBS scheme, as well as in the Odum approach by assigning molecules to the oxidation products. Furthermore, hygroscopicity may be considered in further versions of the VBS, or SVOC can be included in a mechanistic model [Albriet *et al.*, 2010; Couvidat *et al.*, 2012a].

Robinson *et al.* [2007] have shown that some primary organic aerosols (POA) are in fact condensed semi-volatile organic compounds (SVOC), which exist in both the gas phase and the particle phase. Consequently, the amount of POA depends on the dilution of the aerosol, temperature (if the temperature decreases, the volatility of SVOC decreases) and SVOC present in the gas phase, which can be oxidised to form less volatile compounds. The representation of POA in emission inventories (which typically suppose that POA are non-volatile) has therefore been rethought because they are based on PM measurements after some significant dilution of the emissions and do not account for the gaseous fraction of the SVOC present in POA. Couvidat *et al.* [2012a] showed that taking into account the gas-phase fraction of SVOC over Europe increases significantly organic PM concentrations, particularly in winter, in better agreement with observations.

2.2.5 Numerical difficulties linked to modal distributions

Modal models have difficulties to represent the evolution of a mode when it evolves under the effect of different forces that act in different directions. This is particularly true for ultra-fine particles, that is particles of low diameter (less than 100 μm). For example, Sartelet *et al.* [2006] identified a case when the effect of nucleation/condensation and that of coagulation become of the same order of magnitude but act in opposite directions, leading to the splitting of the nucleation mode. This splitting is not reproduced by modal models, which instead predict a broad unimodal distribution centred at a diameter where the real distribution is minimum (Figure 2.4). Although Sartelet *et al.* [2006] built a splitting scheme to reproduce this splitting of the nucleation mode, there may be other cases where modal models have difficulties to represent the evolution of ultra-fine particles. For example, Devilliers *et al.* [2013] show that although modal models perform well when modelling the condensation of sulfate in the case of regional pollution (Figure 2.5), they fail to reproduce the growth of particles from a diesel vehicle exhaust, because of the inability of modal models to handle the Kelvin effect properly (Figure 2.6). They cannot reproduce accurately the growth of a mode when the low-diameter part of the mode shrinks by evaporation because of the Kelvin effect, while the high-diameter part of the mode grows by condensation.

2.3 Cloud droplets

Most particles undergo an hygroscopic growth as relative humidity increases. These particles may act as cloud condensation nuclei (CCN) and they may be activated into cloud droplets. A part of the particle distribution is activated for particles that exceed a critical dry diameter. This

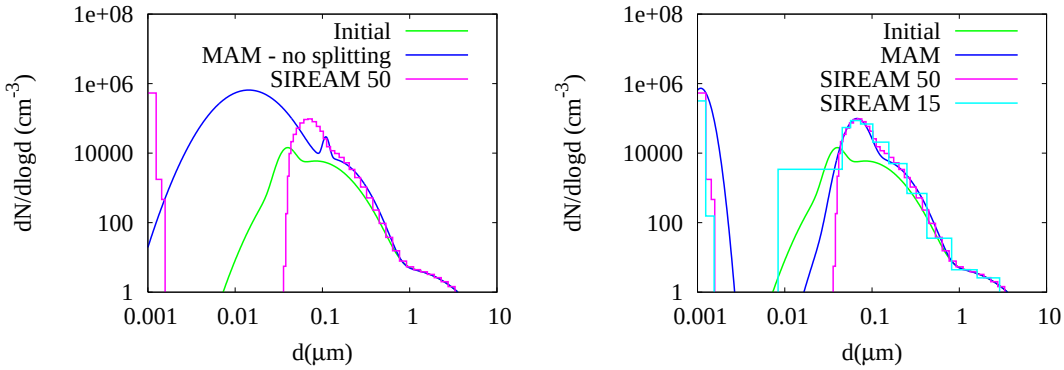

Figure 2.4: Number distribution as a function of particle diameter after 12 h of simulation (nucleation, coagulation, and condensation are taken into account). Left panel: the splitting scheme is not applied in the modal model MAM. Right panel: the splitting scheme is applied in MAM [Sartelet *et al.*, 2006].

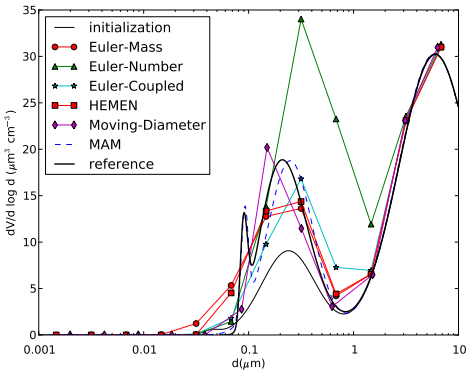

Figure 2.5: Simulation of condensation for the regional pollution case study: volume distribution initially and after 12 hours [Devilliers *et al.*, 2013].

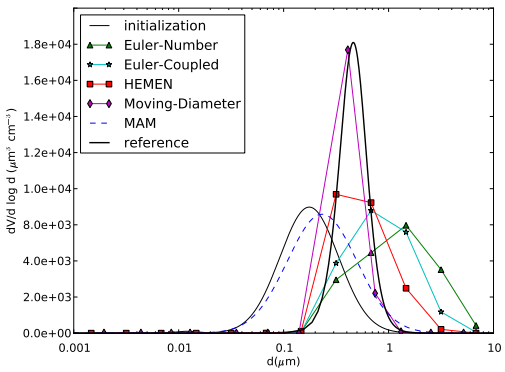

Figure 2.6: Simulation of condensation/evaporation in the diesel exhaust: volume distribution initially and after 1 hour [Devilliers *et al.*, 2013].

critical diameter may be simply estimated using a default value of 0.7 μm [Strader *et al.*, 1998], or using more complex parameterisation [e.g. Abdul-Razzak et Ghan, 2002]. The physical but also to a lesser extent the chemical characteristics of particles may influence the formation of cloud droplets. The chemical composition of the cloud droplet is then given by the activated particle fraction. The water soluble part of the CCN dissolves, and there is mass transfer between atmospheric gases and the cloud droplet. Chemical reactions also take place in the cloud droplet. These reactions are different from the reactions occurring in the particle phase where water is in limited quantity. Aqueous chemical reactions may be represented by chemical schemes such as the one of Pandis et Seinfeld [1989]. Some models start to include SOA formation through cloud processing [Carlton *et al.*, 2008; Couvidat *et al.*, 2012c], by production of low volatility carboxylic acids (e.g., oxalic acid) from precursor water-soluble aldehydes (e.g., glyoxal and methylglyoxal which are formed by the oxydation of isoprene) and by oxidation of methacrolein and methylvinylketone.

2.4 Interaction between the gas and particle phases

The gas and particle phases interact by condensation and evaporation of semi-volatile compounds. However, radicals and less volatile compounds may be affected by the presence of particles via heterogeneous reactions at the aerosol surface and photolysis rates.

Our work in this area has focused on quantitative evaluations of the effects of such interactions on air pollutant concentrations.

2.4.1 Heterogeneous reactions

The heterogeneous reactions at the surface of condensed matter (particles and cloud or fog droplets) may significantly impact gas-phase photochemistry and particles. Heterogeneous reactions for HO_2, NO_2, N_2O_5 and NO_3 at the surface of aerosols and cloud droplets are often modelled following Jacob [2000]:

$$HO_2 \rightarrow 0.5H_2O_2 \tag{2.27}$$
$$NO_2 \rightarrow 0.5HONO + 0.5HNO_3 \tag{2.28}$$
$$NO_3 \rightarrow HNO_3 \tag{2.29}$$
$$N_2O_5 \rightarrow 2HNO_3 \tag{2.30}$$

The chemical composition of particles may influence the surface reaction rates, as shown by Davis *et al.* [2008] for N_2O_5. However, over Europe, Roustan *et al.* [2010] did not find a strong influence of the variations of the N_2O_5 reaction rate with the aerosol composition on nitrate concentrations.

2.4.2 Impact of particles on photolysis rates

Photolysis reactions play a major role in the atmospheric composition. In the troposphere, they drive both O_3 production through NO_2 photolysis, and O_3 destruction through its own photolysis. The photolysis of O_3 is also the main source of OH radicals, which are involved in the formation of secondary aerosols as the main oxidant of their gas precursors.

The photolysis rate coefficient J(i) for a gaseous species i depends on the wavelength λ and can be described as follow:

$$J(i) = \int_{\lambda} \sigma_i(\lambda, P, T)\Phi_i(\lambda, P, T)F(\lambda)d\lambda \tag{2.31}$$

where σ_i and Φ_i are respectively the absorption cross section and the quantum yield of the species i, and F is the actinic flux representative of the irradiance which reaches the level where J is calculated. σ_i and Φ_i are specific to the photolysed species i whereas F depends on the position of the sun but also on the presence of clouds and aerosols.

In an aerosol layer, light beams can be scattered and/or absorbed depending on aerosol optical characteristics, i.e their Optical Properties (OP) at the beam wavelengths, and their Optical Depths (OD) which, given their OP, depend on the aerosol loading. Photolysis rates can be modified by aerosols and clouds inside the layer but also below and above it.

In many chemical-transport models, the impact of aerosols on photolysis rates is not taken into account, while the impact of clouds on photolysis rates is calculated through an attenuation coefficient A_{tt} applied to clear-sky photolysis rate coefficients [Roselle *et al.*, 1999; Sartelet *et al.*, 2007a]. In Real et Sartelet [2011], photolysis rates are computed using the photolysis scheme FAST-J [Wild *et al.*, 2000]. Aerosols and clouds are represented in FAST-J through their optical depths and optical properties at different wavelengths. Fast-J requires the following OP as input of the model: the single scattering albedo, the extinction coefficient and the phase function (expressed as the first 8 terms of its Legendre expansion). For aerosols, these OP are calculated with a Mie model and depend on the aerosol refractive index and aerosol size. For clouds, pre-calculated values of OP are included in Fast-J for several cloud droplet sizes and ice crystal shapes.

Real et Sartelet [2011] compared the impact over Europe with a 0.5° x 0.5° horizontal resolution of taking or not clouds and aerosols into account when computing photolysis rates. R-ATT denotes photolysis rates computed by the attenuation coefficient method, R-COnL (R-AERO) denotes photolysis rates computed by taking into account clouds (clouds and aerosols) in the photolysis scheme.

Mean vertical profiles (averaged over the spatial domain and over the month) of relative differences between NO_2 and O_3 photolysis rate coefficients simulated with R-AERO and R-COnL in July 2001 are shown in Figure 2.7. Relative differences between R-COnL and R-ATT are also shown in order to compare the effects on photolysis rates of changing the cloud parametrisation versus including aerosols. Including the aerosol impact on solar radiation leads to a mean decrease of all photolysis rates (here only NO_2 and JO^1D are shown but other photolysis rates exhibit the same feature) from the ground to 10 km. This decrease is the highest at the ground (-13 to -14 %) and decreases with altitude. At the ground, the impact is much higher than the impact simulated when changing the cloud parametrisation.

2.5 Internal and external mixing

The internal mixing assumption relies on the assumption that particles from different sources mix instantaneously when they are present in the same air mass. Although this assumption may be realistic far from emission sources, it may be difficult to justify close to emission sources, where emitted particles can have compositions that are very different from background particles and from particles emitted from different sources.

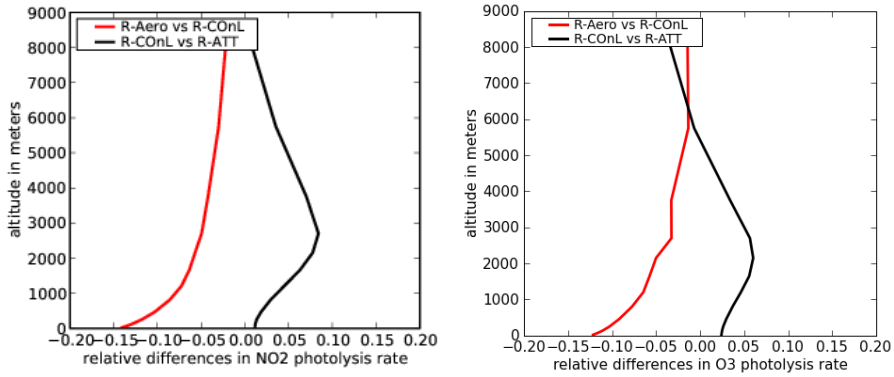

Figure 2.7: Monthly mean vertical profile of relative differences between NO_2 and O_3 photolysis rates simulated with R-ATT, R-COnL and R-AERO for July 2001

Most measurements do not often differentiate between internally and externally mixed particles. However, observations such as those of Mallet *et al.* [2004] for black carbon, Hughes *et al.* [2000] for urban aerosols and Deboudt *et al.* [2010] for African dust show that particles are mostly externally mixed.

Several models have been designed to represent externally mixed particles. Most of them neglect coagulation, because condensation/evaporation is the most crucial process to correctly model the aerosol mass and because coagulation is more difficult to model for an external mixture of particles: when two particles of different compositions coagulate, the resulting particle will have a composition that is different from those of the two particles that have coagulated.

In the Lagrangian and Eulerian models of Kleeman *et al.* [1997] and of Kleeman et Cass [2001], the external mixing assumption is made close to sources, i.e., to each source is associated an aerosol distribution. The different aerosol distributions are then transported in the atmosphere, and they interact with the gas phase by condensation and evaporation. Riemer *et al.* [2009] model externally-mixed particles using a stochastic approach. Although this approach is accurate and takes into account coagulation as well as condensation/evaporation, it is computationally expensive when the number concentration of particles is high. In the models of Jacobson *et al.* [1994] and Lu et Bowman [2010], the coagulated particles can either be internally or externally mixed. In Lu et Bowman [2010], a threshold is used to determine whether the chemical component is internally or externally mixed. For example, if black carbon accounts for more than 5% of the particle mass, then it is internally mixed, else it is externally mixed.

Jacobson [2002] expanded on Jacobson *et al.* [1994] by allowing particles to have different mass fractions, and as an example, the fraction of black carbon in the total particulate mass is discretized. Coagulation interactions are predefined using coefficients which depend on the composition of particless, and if a particle of any mass fraction of BC mixes with a particle of another chemical component, the mass fraction of BC is no longer followed. Oshima *et al.* [2009] used a similar approach, i.e., both the particle size distribution and the fraction of BC in the total particulate mass are discretized into sections, but they did not model coagulation.

The work of Dergaoui *et al.* [2013] further expands these modeling approaches by discretizing and computing the evolution of mass fractions into multiple sections. The particle size distribution and the fraction of any chemical component of particles are discretized into sec-

tions. In other words, the chemical composition of particles in each size section is discretized according to the percentage of one or more of its components. When two particles coagulate, the mass fraction of the resulting particle is computed with coagulation interaction coefficients that depend both on the mass fraction and on the mass of particles.

For the case of s_c species or chemical components, the number concentration is discretised as

$$N^k_{i_1,\,...,\,i_{s_c-1}}(t) = \int_{m_k^-}^{m_k^+} \int_{f_{i_1}^-}^{f_{i_1}^+} ... \int_{f_{i_{s_c-1}}^-}^{f_{i_{s_c-1}}^+} n\left(m, F_1,\ ...., F_{s_c-1}\ , t\right)\, dF_1\, ...\, dF_{s_c-1}\, dm \qquad (2.32)$$

with $k = 1,\ ...,\ s_m$ (s_m is the number of mass sections), $i_1 = 1,\ ...,\ s_{f_1}$ and $i_{s_c-1} = 1,\ ...,\ s_{f_{s_c-1}}$ where s_{f_c} is the number of mass fraction sections for chemical component c.

As an example of the impact of coagulation on the chemical composition of particles, Figure 2.8 shows the number concentration as a function of diameter for particles of different compositions with up to three species. Initially, the particles are assumed not to be mixed, i.e. to be made exclusively of one species. As the mass fraction is discretised with three sections [0, 0.3, 0.7, 1], the mass fraction of non-mixed particles is assumed to be between 0.7 and 1 for one species, while the mass fractions of the other species are between 0 and 0.3. The initial number and mass concentrations used here correspond to the urban conditions of Seigneur et al. (1986). Simulations are conducted for 12 h at a temperature of 298 K and a pressure of 1 atm. After 12 h of simulation, mixing occurs, as shown in Figure 2.8.

Although Dergaoui *et al.* [2013] derived the general dynamic equations for the coagulation of such particle mixtures, they did not model other processes such as condensation/evaporation. Work is ongoing to add those processes and incorporate this treatment of external mixture aerosols with a 3D chemical-transport model (see section 5.1)

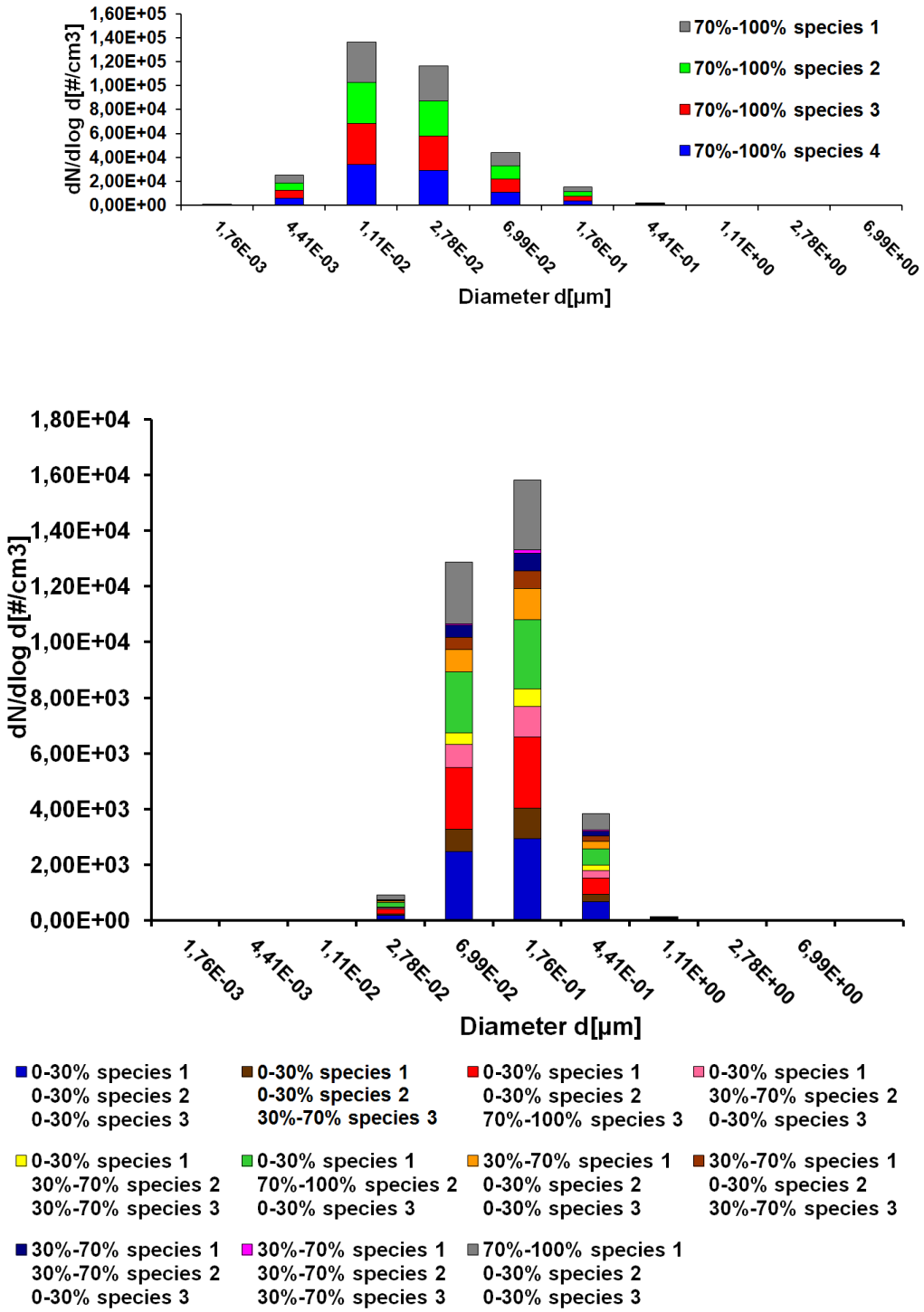

Figure 2.8: Distributions of externally-mixed particles for the case of 3 components: particle number concentration as a function of diameter for particles of different chemical composition. Initial conditions (upper panel) and after 12 h of simulation (lower panel) [Dergaoui *et al.*, 2013].

Chapter 3

Comparison of models to data and model inter-comparisons

In this work, the air quality platform Polyphemus [Mallet *et al.*, 2007] with the air quality model (AQM) Polair3D is used to estimate gaseous and particle concentrations. This chapter describes the model configurations and settings that I have used for different applications. The model is then evaluated by comparisons to ground and lidar data and by model inter-comparisons.

Tables 3.1 and 3.2 compare the different model configurations and settings used in the different studies.

3.1 Model configurations

In Polyphemus, the user can choose between different modules, parameterisations and/or input data. With the Polair3D AQM, different gaseous chemical schemes may be used: RACM [Stockwell *et al.*, 1997], CB05 [Yarwood *et al.*, 2005] or RACM2 [Goliff et Stockwell, 2008]. Heterogeneous reactions are modelled following Jacob [2000]. The aerosol dynamics (coagulation, condensation/evaporation, nucleation) is modelled with the SIze REsolved Aerosol Model SIREAM [Debry *et al.*, 2007]; however the Modal Aerosol Model MAM [Sartelet *et al.*, 2006] was used with Polair3D/RACM over Greater Tokyo and compared to Polair3D/RACM/SIREAM. The thermodynamical model is ISORROPIA [Nenes *et al.*, 1999] for inorganic aerosols, and four secondary organic aerosol (SOA) models may be used: SORGAM, SuperSORGAM [Kim *et al.*, 2011a], MAEC [Kim *et al.*, 2011b] and the Hydrophilic/Hydrophobic Organic model H^2O [Couvidat *et al.*, 2012a]. SORGAM and SuperSORGAM use a standard SOA formulation with hydrophobic absorption of SOA into organic particles. The SOA precursors are aromatics, long-chain alkanes, long-chain alkenes and monoterpenes in SORGAM, while isoprene and sesquiterpenes are also considered in SuperSORGAM with a variation of the biogenic SOA formation depending on the NOx regime. MAEC and H^2O include oxidation of several precursors (aromatics, isoprene, monoterpenes, sesquiterpenes) under several conditions (oxidation under high-NOx and low-NOx conditions) and several processes (condensation into an organic phase or an aqueous phase, oligomerization, hygroscopicity and non-ideality). H^2O also includes the formation of primary SVOC and a more accurate representation of biogenic aerosols: α-pinene and β-pinene are separated and the formation of organo-nitrates from the oxidation of monoterpenes is taken into account.

3.1.1 Aqueous chemistry

For grid cells with a liquid water content exceeding a critical value (the default value is 0.05 g m^{-3}), the cell is assumed to contain a cloud and the aqueous-phase module is called instead of the aerosol module (SIREAM). A part of the particle distribution is activated into cloud droplets, and the evolution of the remaining interstitial particles is not considered. Activation is done for particles that exceed a critical dry diameter, which default value is 0.7 μm [Strader *et al.*, 1998]. The microphysical processes that govern the evolution of cloud droplets are parameterised and not explicitly described. Cloud droplets form on activated particles and evaporate instantaneously (after one numerical timestep) in order to take into account the impact of aqueous-phase chemistry for the activated part of the particle distribution [Fahey et Pandis, 2003]. At the beginning of the time step, the activated particle fraction is incorporated into the cloud droplet distribution. The chemical composition of the cloud droplet is deduced from the activated particle composition. The variable size-resolved model (VSRM) model can simulate a size-resolved droplet distribution, but a bulk approach was used instead in the following simulations in order to decrease the computational time. The average droplet diameter is fixed at 20 μm. Aqueous-phase chemistry and mass transfer between the gaseous phase and the cloud droplets (bulk solution) are then solved. The aqueous-phase model is based on the chemical mechanism developed at Carnegie Mellon University [Fahey et Pandis, 2003; Pandis et Seinfeld, 1989]. This model accounts for 18 gaseous and 28 aqueous species and solves 99 reactions dynamically. Alternatively, a simplified aqueous model may be used. This simple aqueous chemical mechanism only accounts for 15 aqueous and 5 gaseous species, and only solves dynamically 2 reactions (oxidation of S(IV) by ozone and by hydrogen peroxide) [Debry *et al.*, 2007]. At the end of the timestep, the new mass generated from aqueous chemistry is redistributed onto the aerosol bins that were activated.

3.1.2 Land use cover

For land use coverage, either the USGS (United States Geological Survey) land cover map (24 categories) is used, or the Global Land Cover 2000 (GLC2000) database (European Commission, Joint Research Centre, 2003, http://bioval.jrc.ec.europa.eu/products/glc2000/glc2000.php) with 23 categories is used.

3.1.3 Photolysis rates

In the first simulations performed, photolysis rates were computed off-line using the photolysis rate preprocessor JPROC of CMAQ [Roselle *et al.*, 1999]. They are now either computed off-line using tabulations obtained from the photolysis scheme FASTJ [Wild *et al.*, 2000], or computed online every hour using FASTJ. Online computation allows us to take into account the effect of clouds and particles on photolysis rates. When rates are computed off-line, they are multiplied by an attenuation coefficient that parameterises the impact of clouds on photolysis rates.

3.1.4 Dry and wet deposition

The dry deposition velocities of gases are preprocessed using the parameterisation of Zhang *et al.* [2003]. As in Simpson *et al.* [2003], the surface resistance is modelled following Wesely [1989]

for sub-zero temperatures, and the surface resistance of HNO_3 is assumed to be zero for positive temperatures. Below-cloud scavenging (washout) is parameterised following Sportisse et Dubois [2002]. During below-cloud scavenging, concentrations of soluble gaseous species can be significantly affected by the ion dissociation during dissolution in water. To take this ionisation process into account, given the raindrop pH, effective Henry's law coefficients are computed for the following species: SO_2, NH_3, HNO_3, HNO_2 and HCl.

For particles, dry deposition is parameterised with a resistance approach, following Zhang *et al.* [2001]. Below-cloud scavenging is parameterised with the washout coefficient

$$\Lambda(d_p) = \frac{3}{2} \frac{E(D_r, d_p)\, p_0}{D_r} \tag{3.1}$$

with p_0 the rain intensity, d_p the particle diameter, D_r the raindrop diameter and E the collision efficiency. The representative diameter for the rain is given as a function of p_0 following Loosmore et Cederwall [2004]. The raindrop velocity is computed as a function of the raindrop diameter following Loosmore et Cederwall [2004].

In-cloud scavenging (rainout) is parameterised following Roselle et Binkowski [1999]. In the case of a fog in the first layer (diagnosed when the grid cell liquid water content is larger than a critical value of 0.05 g m^{-3}), the fog settling velocity is parameterised following Pandis *et al.* [1990].

3.1.5 Meteorology: vertical diffusion

Meteorological fields are computed off-line, i.e. they are computed separately from the air quality simulation with the AQM. For example, they may be obtained from ECMWF (European Centre for Medium-Range Weather Forecasts), from the models MM5 (the PSU/NCAR mesoscale model) or WRF (the Weather Research and Forecasting Model). Vertical diffusion may be recomputed in a preprocessing stage of the CTM, using the Troen and Mahrt (TM) parameterisation (Troen et Mahrt [1986]) within the boundary layer. Alternatively, the Louis parameterisation may also be used as in Roustan *et al.* [2010]. Kim *et al.* [2013] use the vertical diffusion directly estimated from the parameterisations in WRF.

3.2 Model settings

3.2.1 Over Europe

3.2.1.1 Domain

Over Europe, two domains are used. The smaller domain is (34.75° N - 57.75° N; 10.75° W - 22.75° E). The larger domain, which covers the whole of Europe, is (35° N - 70° N; 15° W - 35° E). The horizontal step is 0.5° along both longitude and latitude, except for the inter-comparison study AQMEII (Air Quality Modelling Evaluation International Initiative), where a step of 0.25° was used for consistency with the other models included in the inter-comparison.

The number of vertical levels varies from 5 to 28 depending on the application. Even when a small number of vertical levels is used in the AQM, e.g. 5 to 10, a larger number of vertical levels is used to compute meteorological fields.

3.2.1.2 Boundary conditions

For boundary conditions, daily means are extracted from outputs of global Chemical- Transport Models. Sartelet *et al.* [2007a]; Kim *et al.* [2009, 2011b]; Real et Sartelet [2011]; Roustan *et al.* [2010] used outputs from Mozart 2 simulations over a typical year for gases, and outputs from the Goddard Chemistry Aerosol Radiation and Transport [Chin *et al.*, 2000, GOCART] model for the year 2001 for sulfate, dust, black carbon and organic carbon. Couvidat *et al.* [2012a] used boundary conditions for particles from ECHAM5-HAMMOZ [Pozzoli *et al.*, 2011]. In Sartelet *et al.* [2012], boundary conditions are the default AQMEII conditions provided by the GEMS (Global Earth-system Monitoring using Satellite and in-situ data) project. In Kim *et al.* [2013], boundary conditions are daily outputs of the global chemistry and aerosol model, Interaction Chimie-Aérosols (INCA) coupled to the Laboratoire de Météorologie Dynamique general circulation model (LMDz) for the year 2005 (http: //www-lsceinca.cea.fr/).

3.2.1.3 Emissions

Anthropogenic emissions are obtained from emission inventories. Over Europe, the EMEP (European Monitoring and Evaluation Programme, www.emep.int) expert inventory with a resolution of 0.5° x 0.5° is often used, although Sartelet *et al.* [2012] also use anthropogenic emissions from TNO (www.tno.nl). A typical time distribution of emissions, given for each month, day and hour [e.g. GENEMIS, 1994] is then applied to each emission sector or SNAP (Selected Nomenclature for Air Pollution) category. The inventory species are disaggregated into real species using speciation coefficients [e.g. Passant, 2002, over Europe]. The real species are thereafter aggregated into the model species. Primary particle emissions are usually given in total mass. These raw data are chemically speciated and size seggregated by SNAP category or emission source [e.g. Simpson *et al.*, 2003].

Over Europe, biogenic emissions are computed as in Simpson *et al.* [1999]. Two thirds of terpene emissions are allocated to α-pinene and one third to limonene [Johnson *et al.*, 2006]. Alternatively, biogenic emissions can be computed using the Model of Emissions of Gases and Aerosols from Nature with the EFv2.1 dataset [MEGAN, Guenther *et al.*, 2006]. The two biogenic emission schemes use different methodologies: MEGAN uses canopy-scale emission factors based on leaf area index obtained from the standard MEGAN LAIv database [MEGAN-L, Guenther *et al.*, 2006], whereas Simpson uses leaf-scale emission factors based on GLC2000 land-use categories. Furthermore, although terpene emissions are distributed amongst pinene, limonene and sesquiterpenes with constant factors, different emission factors are used for several species in MEGAN.

Sea-salt emissions are parameterised following Monahan *et al.* [1986], who model the generation of sea-salt by the evaporation of sea spray produced by bursting bubbles during whitecap formations due to surface wind. This parameterisation is valid at 80% relative humidity. To generalise it, the formula is expressed in terms of dry radius, which is assumed to be approximatively half the radius at 80% humidity [Gerber, 1985]. The emitted mass of sea-salt is assumed to be made of 55.025% of chloride, 30.61% of sodium and 7.68% of sulfate [Seinfeld et Pandis, 1998].

3.2.2 Over North America

In the framework of the AQMEII project, simulations were performed over North America. Over North America, the horizontal domain was (24°N-53.75°N; 125.5°W-64°W) with a horizontal resolution of 0.25° x 0.25° and 9 vertical levels. The meteorological data correspond to the default WRF data provided for the AQMEII inter-comparison [Vautard *et al.*, 2012]. Anthropogenic, biogenic from BEIS3.14 and biomass burning emissions were those provided by US-EPA for AQMEII [Pouliot *et al.*, 2012].

3.2.3 Over East Asia

In the framework of the Model InterComparison Study of atmospheric dispersion models for Asia (MICS-Asia) project, simulations were performed over East Asia. The domain was (19.7°N - 48.8°N; 88.6°E - 150.4°E) with a horizontal resolution of 45 km and 9 vertical levels. All the models of the MICS project used a common data set for anthropogenic and biomass burning emissions from Streets *et al.* [2003]. The volcanic emission was derived from Kajino *et al.* [2004]. The release heights were prescribed at an altitude of about 300 m for large point source and 1500 m for volcanic emission. Natural emissions (biogenic VOCs, soil and lighting NOx, dust) were not specified. Sea-salt emissions were parameterised following Monahan *et al.* [1986], as done over Europe. Most MICS models use a common data source for boundary conditions, which was derived from a global AQM, namely MOZART-II [Holloway *et al.*, 2008]. Meteorological fields were derived from MM5.

3.2.4 Over Greater Paris

3.2.4.1 Domain

To simulate air quality over Greater Paris, 3 nested simulations were performed: Europe, France and Greater Paris. In Royer *et al.* [2011]; Couvidat *et al.* [2012b], the horizontal domain is (35 - 70° N; 15° W - 35° E) with a resolution of 0.5° x 0.5° over Europe (it corresponds to the largest domain of section 3.2.1.1), the domain is (41 - 52° N; 5° W - 10° E) with a resolution of 0.1° x 0.1° over France and (47.9 - 50.1° N; 1.2° W - 3.5° E) with a resolution of 0.02° x 0.02° over Greater Paris. In Kim *et al.* [2013], three nested simulations are also performed. The European domain is the same as in Royer *et al.* [2011]. The first nested domain covers France with a resolution of 0.125° x 0.125° (41.5°N - 51.1°N, 4.0°W - 10.1°E) and the smallest domain covers Greater Paris with a resolution of 0.02° x 0.02° (48.1°N - 49.2°N, 1.4°E - 3.5°E).

3.2.4.2 Boundary conditions

Boundary conditions for the largest domain (European domain) are the same as described in section 3.2.1.2. For the other two sub-domains (France and Greater Paris), boundary conditions are obtained from the simulation on the larger domain.

3.2.4.3 Emissions

Over Europe and France, the EMEP expert inventory is used. Over Greater Paris, anthropogenic emissions are generated with the AIRPARIF inventory for 2000 or 2005 where available and

with the EMEP expert inventory elsewhere. The NMVOC are distributed in real species using the speciation of the Institut für Energiewirtschaft und Rationelle (IER), Stuttgart, then allocated to model species. PM_{10} and $PM_{2.5}$ are distributed in size, following the EMEP recommendations, and the chemical speciation of PM corresponds to the one estimated for Milan in the framework of the CityDelta project (http://aqm.jrc.it/citydelta/).

3.2.5 Over Greater Tokyo

Simulations were performed over a 210 km x 240 km area, centred around Tokyo, with a 5 km x 5 km resolution (Figure 1 shows the domain of simulation, which is discretised with 42 x 48 points). 12 vertical levels are considered (0, 29, 58, 103, 147, 296, 447, 677, 954, 1282, 1705, 2193, and 2761 m).

Meteorological data were provided by the Japanese Meteorological Agency with a 20 km x 20 km resolution every 6 h. Finer hourly meteorological data, with a 5 km x 5 km resolution were obtained by running the meteorological model MM5, the Fifth-Generation Pennsylvania State University/ National Center for Atmospheric Research (NCAR) Mesoscale model. Initial and boundary conditions (with inputs varying every 3 h) were obtained by running the Community Multi-scale Air Quality (CMAQ) model over East Asia with a 45 km x 45 km resolution. Emission inventories were provided by a collaboration with the Japanese National Institute for Environmental Studies. Emission sources include mobile sources (road, air, and vessels), stationary sources (domestic and industries), wastewater treatment, and biogenic/natural sources (agriculture, soil, and volcanoes). The size distribution and the chemical speciation of PM_{10} and $PM_{2.5}$ were specified as in CMAQ [Binkowski et Roselle, 2003]. All PM_{10} - $PM_{2.5}$ are assigned to the coarse mode and particles are assumed to be made of 90% dust and 10% elementary carbon. Most of $PM_{2.5}$ (99.9%) are assigned to the accumulation mode and 0.1% to the Aitken mode. For $PM_{2.5}$, primary particles are assumed to be made of 30% dust and 70% elementary carbon.

Reference	[1]	[2]	[3]	[4]	[5]	[6]	[7]	[8]
Domain	Europe	Europe	Europe	Europe	Europe	Europe	Europe	Europe
Gas Chemistry	RACM	CB05/RACM2	RACM	RACM	CB05/RACM2	CB05/RACM2	RACM	CB05
PM dynamics	SIREAM	SIREAM	SIREAM	SIREAM	SIREAM	SIREAM	SIREAM	SIREAM
SOA	Sorgam	–	Sorgam	Sorgam	MAEC	Sorgam/MAEC SuperSorgam	SuperSorgam	H^2O
LUC	USGS	USGS	USGS	USGS	USGS	USGS	GLC2000	USGS
Photolysis	JPROC off-line	FASTJ off-line	JPROC off-line	FASTJ on/off-line	FASTJ off-line	FASTJ off-line	FASTJ off-line	FASTJ off-line
Ant. em.	EMEP	EMEP	EMEP	EMEP	EMEP	EMEP	EMEP/TNO	EMEP/[9]
Bio. em.	Simpson	Simpson	Simpson	Simpson	Simpson	Simpson	Simpson /MEGAN	MEGAN
Meteorology	ECMWF	ECMWF	ECMWF	ECMWF	ECMWF	ECMWF	MM5	ECMWF
Vert. diff.	TM	TM	TM Louis	TM	TM	TM	TM	TM
Bound. cond.	MOZART GOCART	MOZART	MOZART GOCART	MOZART GOCART	MOZART GOCART	MOZART GOCART	GEMS	MOZART HAMMOZ
Vertical levels	5 0 to 3 km	5 0 to 3 km	5 or 10 0 to 3 km	13 0 to 10 km	5 0 to 3 km	5 0 to 3 km	9 0 to 12 km	9 0 to 12 km

Table 3.1: Comparisons of the different model configurations and settings used in the different studies over Europe. [1]: Sartelet *et al.* [2007a], [2]: Kim *et al.* [2009], [3]: Roustan *et al.* [2010], [4]: Real et Sartelet [2011], [5]: Kim *et al.* [2011b], [6]: Kim *et al.* [2011a], [7]: Sartelet *et al.* [2012], [8]: Couvidat *et al.* [2012a], [9]: Junker et Liousse [2008]

Reference	[9]	[10]	[11]	[12]	[13]	[14]
Domain	Paris	Paris	Paris	East Asia	Tokyo	North America
Gas Chemistry	RACM	CB05	CB05	RACM	RACM	CB05
PM dynamic	SIREAM	SIREAM	SIREAM	SIREAM	MAM/SIREAM	SIREAM
SOA	AEC	H^2O	AEC	–	–	SuperSorgam
LUC	GLC2000	USGS/Corine	USGS/Corine	USGS	USGS	GLC2000
Photolysis	FASTJ	FASTJ	FASTJ	JPROC	JPROC	FASTJ
	off-line	off-line	off-line	off-line	off-line	on-line
Ant. em.	Airparif	Airparif	Airparif	Street	NIES	US-EPA
Bio. em.	Simpson	Simpson	Simpson	–	–	BEIS
Meteorology	MM5	WRF-urban	WRF-urban	MM5	MM5	WRF
Vert. diff.	TM	TM	TM + WRF	TM	TM	TM
Boundary cond.	Polair3d Europe	Polair3d Europe	Polair3d Europe	CMAQ	CMAQ	GEMS
Vertical levels	9	9	29	9	12	9
	0 to 12 km	0 to 12 km	0 to 13 km	0 to 5.5 km	0 to 5 km	0 to 12 km

Table 3.2: Comparisons of the different model configurations and settings used in the different studies (outside Europe). [9]: Royer *et al.* [2011], [10]: Couvidat *et al.* [2012b], [11]: Kim *et al.* [2013], [12]: Sartelet *et al.* [2008], [13]: Sartelet *et al.* [2007b], [14]: Sartelet *et al.* [2012]

3.3 Comparison to surface data

To evaluate AQM simulations by comparison to ground data, the following statistics are commonly computed: root mean square error (rmse), mean fractional error (mfe), mean fractional bias (mfb), normalised mean bias (nmb), normalised mean error (nme) and correlation coefficient (r). For O_3, the mean normalised gross error (mnge) and mean normalised gross bias (mngb) are computed with a cutoff, usually of about 80 μg m^{-3} (i.e. about 40 ppb). Russell et Dennis [2000] recommend performance criteria for hourly O_3 to be |mngb| $\leq$ 15% and mnge $\leq$ 30%. For PM, Boylan et Russell [2006] and Yu *et al.* [2006] have proposed model performance criteria. Boylan et Russell [2006] propose that a model performance goal is met for PM when both the mfe is less than or equal to +50% and the mfb is within $\pm$30% respectively, and a model performance criterion is met when both mfe $\leq$ +75% and $-60\% \leq$ mfb $\leq$ 60%. Yu *et al.* [2006] proposes a model performance criterion is met for sulfate when |nmb| $\leq$ 25% and nme $\leq$ 35%. The metrics used by Boylan et Russell [2006] give the same weight to all concentrations, while the metrics used by Yu *et al.* [2006] are largely influence by high concentrations.

Over Europe, the model results are compared to observational data provided by three databases:

- the EMEP database, available on the EMEP Chemical Co-ordinating Centre (EMEP/CCC) web site at `http://www.emep.int`;
- the AirBase database, available on the European Environment Agency (EEA) web site at `http://air-climate.eionet.europa.eu/databases/airbase`;
- The BDQA database ("Base de Données Qualité de l'Air": the French Data Basis for Air Quality that covers France).

The measurement sites of the EMEP network are assumed to be representative of regional background concentrations. The AirBase database contains observational data from the European Air Quality monitoring network (EuroAirnet). For our comparisons, only the stations labelled as "background" representative have been used. However, it should be kept in mind that "background" does not have exactly the same meaning between AirBase and EMEP. For instance traffic and industrial stations have been excluded but stations representative of urban or suburban background have been kept. The same kind of filter has been applied to data from the BDQA, "rural" and "suburban" stations have been retained. The measurement data for nitrate, ammonium and OC are limited to a few measurement stations (14 stations) and only to the years 2002-2003 for OC.

Over Greater Paris, measurements from Airparif are used (http://www.airparif.fr/). They are included in the BDQA database. The number of stations used for the measurements are more numerous for O_3 (about 30) than for PM_{10} (about 17) and $PM_{2.5}$ (about 5).

Over East Asia, measurement comparisons are presented for nitrate and sulfate compounds. They are available at only three stations from the Acid Deposition Monitoring Network in East Asia (EANET) and at Fukue Island, a remote site between Japan and China. Although daily mean concentrations are measured at Fukue, monthly mean concentrations are measured at EANET stations.

Over Tokyo, simulations were performed for highly polluted days. Measurements of $PM_{2.5}$ chemical compounds are available at four sites for 9-10 December 1999, and at 2 sites for 31 July-1 August 2001.

Tables 3.3 and 3.4 compares the different statistics used in the different studies over Europe and over domains other than the European domain respectively.

For O_3, the model performance criteria are globally satisfied, although the mngb is sometimes higher in absolute value than 15% when the chemical scheme RACM is used. However, the bias is lower than 15% when using CB05 or RACM2 and the model performance criteria is verified over Europe as well as over Paris or North America.

For PM_{10} and $PM_{2.5}$, the model performance criteria of Boylan et Russell [2006] is always met, although the model performance goal is not depending on the place, season and the observational data network used for the comparison. For example, over Europe, for the year 2001, the model performance goal is met for the EMEP network but not for the Airbase network for which PM_{10} is largely underestimated. These differences stress the importance of the filtering of the stations used for the comparisons. The differences originate from the station types: EMEP includes mostly rural background, while Airbase includes as well suburban and urban background. As a consequence, the concentrations observed at EMEP stations are lower than those observed at AirBase stations. Over North America during summer 2006, the model performance goal is not met for PM_{10} but it is met for $PM_{2.5}$ suggesting some missing primary aerosol sources.

For sulfate (PSO_4), the model performance criteria of Boylan et Russell [2006] is always met. The model performance criteria of Yu *et al.* [2006] is met over Tokyo and East Asia. Over Europe, the nme is too large, although the bias is low. For ammonium, the model performance criteria of Boylan et Russell [2006] is met most of the time: during the year 2001 over Europe and during summer 2006 over North America. However, ammonium is over-estimated during summer 2006 over Europe. For nitrate, the results are not as good as for sulfate and ammonium, but the model performance criteria of Boylan et Russell [2006] is met for the year 2001, although it is not for 2006 over Europe and North America. Over East Asia, the nme of the model performance criteria of Yu *et al.* [2006] vary greatly depending on the simulations, and over Europe and Tokyo the model performance criteria of Yu *et al.* [2006] are not met for nitrate and ammonium. These criteria were defined for sulfate which is less volatile than nitrate and ammonium, and therefore easier to model, i.e. with less uncertainty. For OC, the model performance criteria of Boylan et Russell [2006] are met both over Europe for the years 2002/2003 and over North America for the summer 2006.

References			[1]	[2] and [5]	[3]		[4]		[7]	[8]
Time period			1 year	Summer	Summer	Winter	Summer	Winter	Summer	1 year
O_3	EMEP	mnge/mngb	22/-18							
	BDQA	mnge/mngb	20/-16							
	Airbase	mnge/mngb	20/-16						23.1/-18.7	
PM_{10}	EMEP	mfe/mfb	50/-7	40/-22						
		nme/nmb			33.9/-25.2	56.7/-23.8				
	BDQA	mfe/mfb	40/-25							
	AirBase	mfe/mfb	58/-42						46.3/-9.0	
		nme/nmb					42.0/-36.0	64.6/21.0		
$PM_{2.5}$	EMEP	mfe/mfb	61/-39	39/-7						
		nme/nmb			32.9/-3.8	52.8/-25.1				
	AirBase	mfe/mfb							57.4/28.9	
PSO_4	EMEP	mfe/mfb	50/-4	45/-0.1					53.7/31.7	
		nme/nmb			48.0/-3.7	63.5/-2.4				
PNO_3	EMEP	mfe/mfb	75/32	72/-11					108.2/-13.1	
		nme/nmb			77.9/-7.1	78.6/-16.5				
PNH_4	EMEP	mfe/mfb	50/20	43/10					91.2/75.7	
		nme/nmb			39.8/-9.3	58.3/-26.5				
OC	EMEP	mfe/mfb								50/-37

Table 3.3: Comparisons of the different statistics obtained in the different studies over Europe in %. [1]: Sartelet *et al.* [2007a], [2]: Kim *et al.* [2009], [3]: Roustan *et al.* [2010], [4]: Real et Sartelet [2011], [5]: Kim *et al.* [2011b], [7]: Sartelet *et al.* [2012], [8]: Couvidat *et al.* [2012a]. For [2], [3], [5] and [8], the performance of the best model configuration (in terms of nme) is presented for each pollutant.

References		[9]	[10]	[11]	[12]	[13]	[14]
Time period		July 2009	July 2009	May 2005	4 months 2001/2002	Dec 1999 July 2001	Summer 2006
Domain		Paris	Paris	Paris	East Asia	Tokyo	North America
O_3	mnge/mngb		15.4/-4.2	14/0			25.6/3.8
PM_{10}	mfe/mfb	mfe: 32.5		40/-9			67.5/-49.4
$PM_{2.5}$	mfe/mfb		39/-9	41/-1			47.7/23.1
PSO_4	mfe/mfb						54.8/-8.1
	nme/nmb				nme: 12	33/26 32/11	
PNO_3	mfe/mfb						129.3/-32.6
	nme/nmb				nme: 20	58/-10 45/4	
PNH_4	mfe/mfb						62.9/28.8
	nme/nmb					56/5 49/-30	
OC	mfe/mfb						72.1/41.5
EC	mfe/mfb						56.5/23.6

Table 3.4: Comparisons of the different statistics obtained in the different studies (outside Europe) in %. [9]: Royer *et al.* [2011], [10]: Couvidat *et al.* [2012b], [11]: Kim *et al.* [2013], [12]: Sartelet *et al.* [2008], [13]: Sartelet *et al.* [2007b], [14]: Sartelet *et al.* [2012]. For [11] and [12], the performance of the best model configuration (in terms of nme) is presented for each pollutant.

3.4 Comparison to lidar data

Thanks to the new generation of portable lidar systems developed in the past five years, accurate vertical profiles of aerosols can now be measured [Raut et Chazette, 2007, 2009]. Such instruments document the mid and lower troposphere by means of aerosol optical properties. Lidar measurements were used in several campaigns, such as LISAIR (LIdar pour la Surveillance de l'AIR) in May 2005 over Paris [Raut et Chazette, 2007], MEGAPOLI (Megacities: Emissions, urban, regional and Global Atmospheric POLlution and climate effects, and Integrated tools for assessment and mitigation) summer experiment in July 2009 over Paris [Royer *et al.*, 2011] and during the eruption of the Icelandic volcano Eyjafjallajökull on 14 April 2010 [Chazette *et al.*, 2012].

The ground-based mobile lidar (GBML) used during the MEGAPOLI and LISAIR campaigns is based on a lidar commercialised by the LEOSPHERE company and initially developed by the Commissariat à l'Energie Atomique (CEA) and the Centre National de la Recherche Scientifique (CNRS). This instrument was taken on board a van with a power supply delivered by batteries giving an autonomy of about 3 h 30 min.

This system is particularly well-adapted to air pollution and tropospheric aerosol studies thanks to its full overlap reached at about 150-200m height and its high vertical resolution of 1.5 m. It is based on a laser delivering 6 ns width pulses at the repetition rate of 20 Hz with a mean pulse energy of 16 mJ at 355 nm. The detection is realized with photo-multiplier tubes and narrowband filters with a bandwidth of 0.3 nm. The final vertical resolution of the data is 15 m after filtering for a temporal resolution of 20 s. The lidar gives access to the aerosol optical properties (e.g. extinction coefficient in synergy with sun-photometer measurements) and the atmospheric structures (planetary boundary layer (PBL) height, aerosol and cloud layers).

Raut et Chazette [2009] established an empirical relation between mass concentration and optical properties of pollution aerosols for urban, peri-urban and rural environments over the Île-de-France region. Thereby, the PM_{10} concentrations above the Paris urban area can be retrieved from the ground-based lidar system with an uncertainty of about 25%. Royer *et al.* [2011] generalises this relation to cases of wet particles (RH above the point of deliquescence), by assuming that the size, mass and optical properties of particles grow following the relations given by Hänel [1976].

During the MEGAPOLI summer campaign GBML was used to perform measurements along and across the pollution plume emitted by Paris and its suburbs. By comparison to ground measurements from Airparif (BDQA network), on average over the 10 different measurement days, the model satisfies the criterion of Boylan et Russell [2006] for the mfe of PM_{10} (= 32.5%).

The most polluted days are 1 and 16 July 2009. The most polluted day, 1 July 2009 is characterised by high surface temperatures (up to 30°C) and anti-cyclonic conditions. As shown in Figure 3.1, lidar measurements are performed leeward inside the pollution plume southwest of Paris from Saclay (latitude 48.73°N; longitude 2.17°E) to Chateaudun (latitude 48.1°N; longitude 1.34°E) between 12 :48 and 15 :58 local time (LT). On 16 July 2009, GBML measurements are performed north of Paris from Saclay (latitude 48.73°N; longitude 2.17°E) to Amiens (latitude 49.89°N; longitude 2.29°E) between 13 :00 to 16 :30 LT. The comparisons of modelled PM_{10} concentrations to those deduced from lidar measurements using urban, peri-urban and rural parameterisations are shown in Figure 3.2. The comparison between simulated PM_{10} concentrations to those deduced from GBML measurements satisfies the criterion

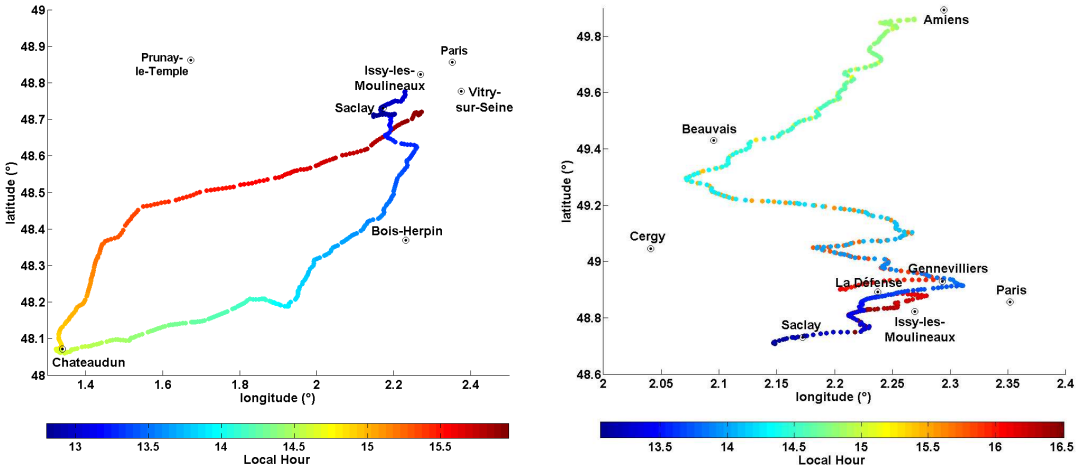

Figure 3.1: Lidar van-circuits performed during the MEGAPOLI summer experiment for the 1 (left panel) and 16 (right panel) July 2009. The colour scale indicates the decimal hours in LT [Royer *et al.*, 2011].

of Boylan et Russell [2006] for the MFE. Wet PM_{10} between GBML with peri-urban relationship and models have shown the following error statistics in terms of rmse (mfe): 8.2 μg.m^{-3} (13.4%) on 1 July, and 5.1 μg.m^{-3} (24.9%) on 16 July.

Lidar data are also used to estimate the PBL height. A GMBL was used during the air quality observation campaign LISAIR over Greater Paris from 24 May to 27 May 2005 [Raut et Chazette, 2009]. The accurate heights of the limits between the multiple layers are obtained from an algorithm enabling the detection of vertical heterogeneity in the aerosol extinction coefficients derived from lidar profiles [Kim *et al.*, 2013]. Figure 3.3 shows the routes taken for the measurements of the GBML, and Figure 3.4 shows the boundary-layer heights estimated by the GBML and modelled heights. Modelled heights are obtained from different simulations of WRF over Greater Paris, using different parameterisations of the PBL height (ACM2, MYJ, MYNN, YSU in Figure 3.4) and including or not urban anthropogenic heat release (with or without the urban canopy model in WRF in Figure 3.4). The PBL heights tend to be underestimated, although the modelled mean PBL heights are significantly different among the PBL schemes. For measurements along the main road and the beltway of Paris, the PBL heights are better estimated when urban anthropogenic heat release is taken into account.

3.5 Model inter-comparisons

Model performances are checked using criteria detailed in Section 3.3. However, the performances may strongly vary depending on the locations and episodes. For a particular episode and location, it is useful to compare the performances of different models, in order to check that a model performs reasonably well. Multi models simulations also enable ensemble modelling [Solazzo *et al.*, 2012b].

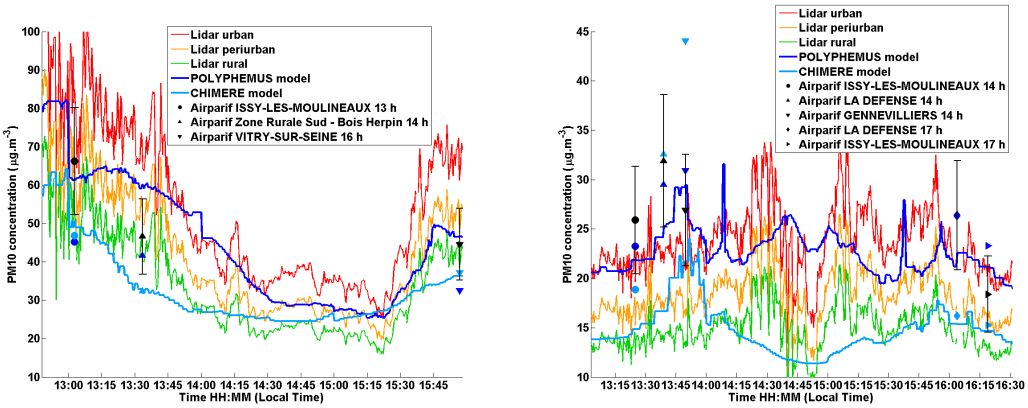

Figure 3.2: Comparison for 1 (left panel) and 16 (right panel) July 2009 of wet PM_{10} derived from GBML using urban (red curves), peri-urban (orange) and rural relationships (green) at 210 m, and wet PM_{10} extracted from POLYPHEMUS model at 210 m (in dark blue) and CHIMERE model at 250 m (in light blue). AIPARIF dry PM_{10} are indicated by black symbols for the nearest stations (located at less than 10 km from GBML) and dry PM_{10} modelled at the lowest level are indicated with dark blue (for POLYPHEMUS) and light blue (for CHIMERE) filled symbols [Royer *et al.*, 2011].

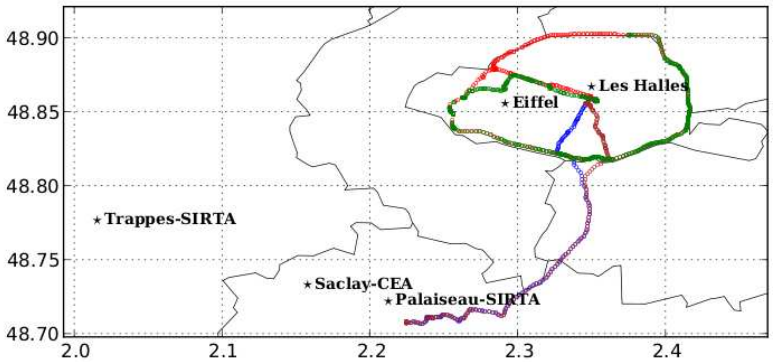

Figure 3.3: Locations of routes taken for the measurements of the GBML. Blue and brown marks show the route for the measurements from the suburbs of Paris to Paris centre for 24 May and 25 May, respectively. Red ones are for the measurements on the beltway of Paris before rush-hour and green ones are for the measurements on the beltway during rush-hour for 25 May 2005 [Kim *et al.*, 2013].

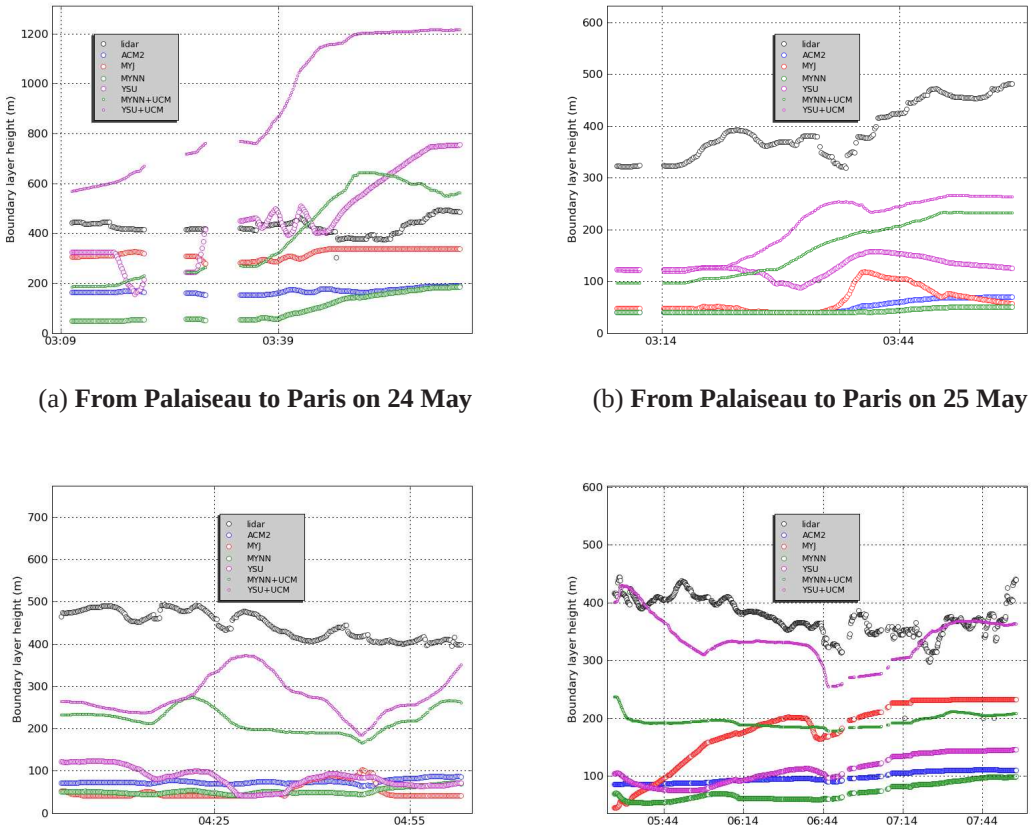

(a) **From Palaiseau to Paris on 24 May**

(b) **From Palaiseau to Paris on 25 May**

(c) **Main road and the beltway of Paris before rush-hour on 25 May**

(d) **Main road and the beltway of Paris during rush-hour on 25 May**

Figure 3.4: Boundary-layer heights estimated by the GBML and modelled heights using different parameterisations of the PBL height (ACM2, MYJ, MYNN, YSU) and including or not urban anthropogenic heat release (with or without the urban canopy model in WRF) [Kim *et al.*, 2013].

3.5.1 Over East Asia: MICS

In the Model InterComparison Study Asia Phase II (MICS-Asia II) [Carmichael *et al.*, 2008], nine different regional modelling groups simulated chemistry and transport of ozone [Han *et al.*, 2008], secondary aerosol [Hayami *et al.*, 2008], acid deposition [Wang *et al.*, 2008], using common emissions and boundary conditions [Holloway *et al.*, 2008] derived from a global model (MOZART, v. 2.4).

These included: a model from Seoul National University [Chang et Park, 2004]; the PATH model from Hong Kong Environmental Protection Department; the RAQM model from the Acid Deposition and Oxidant Research Center, Japan [Han *et al.*, 2004]; the MSSP model from Disaster Prevention Research Institute, Kyoto University [Kajino *et al.*, 2004]; the STEM model from the Center of Global and Regional Environmental Research (CGRER), Iowa University [Carmichael *et al.*, 2003]; the MATCH model from the Swedish Meteorological and Hydrological Institute; the Polair3D model from the Centre d'Enseignement et de Recherche en Environnement Atmospherique (CEREA), France; and two applications of the CMAQ model (http:// www.epa.gov/asmdnerl/CMAQ/): one by the Central Research Institute of the Electric Power Industry, Japan, and the other one by the University of Tennessee, USA.

These models differ in the chemical mechanisms used, the details of aerosol processes, as well as in the coordinate systems and numerical schemes.

Four-month-long periods, representing 2 years and three seasons (i.e., March, July, and December 2001, and March 2002), are analysed. Observational data, obtained under the EANET (the Acid Deposition Monitoring Network in East Asia) monitoring program (see Figure 3.6), were made available for this study, and these data provide a regional database to compare with model simulations. Comparisons for O_3 are shown in Figure 3.5. Most stations with O_3 measurements are in Japan. In terms of statistics, M6, M7 and M8 exhibit notably larger correlations and smaller RMSE than the rest, but all models tend to under-predict monthly average ground-level O_3 levels, with the mean bias error being -2.2 to -18.8 ppbv ([Han *et al.*, 2008]). For daily concentrations, the O_3 observations are measured at only six Japanese sites. All models show a tendency to under-predict O_3 by 4-36%, with an exception of M1, which over-predicts O_3 by 6%. M5 was run only for March 2001, and it is the only model that over-predicts O_3 during that period, which could be associated with the altitudinal difference between the lowest model layer (about 75m in M5 and 10-20m in other models) or its relatively coarse grid resolution both in horizontal and vertical extensions.

Model-observation comparisons were made with monthly-mean measurements of sulfate, total nitrate and total ammonium at EANET stations and daily measurements of sulfate and nitrate at Fukue, a remote site between Japan and China [Hayami *et al.*, 2008]. The comparison of monthly-mean measurements at EANET stations are shown in Figure 3.7. Total nitrate was consistently and considerably underestimated by all the models. At Fukue, the models showed better agreement than for EANET measurements. This is likely because Fukue is centred in many of the model domains, whereas the EANET stations are mostly in Southeast Asia and Russia. Moreover, Fukue is in Northeast Asia, where emissions are high and the emission inventory is more reliable than in Southeast Asia.

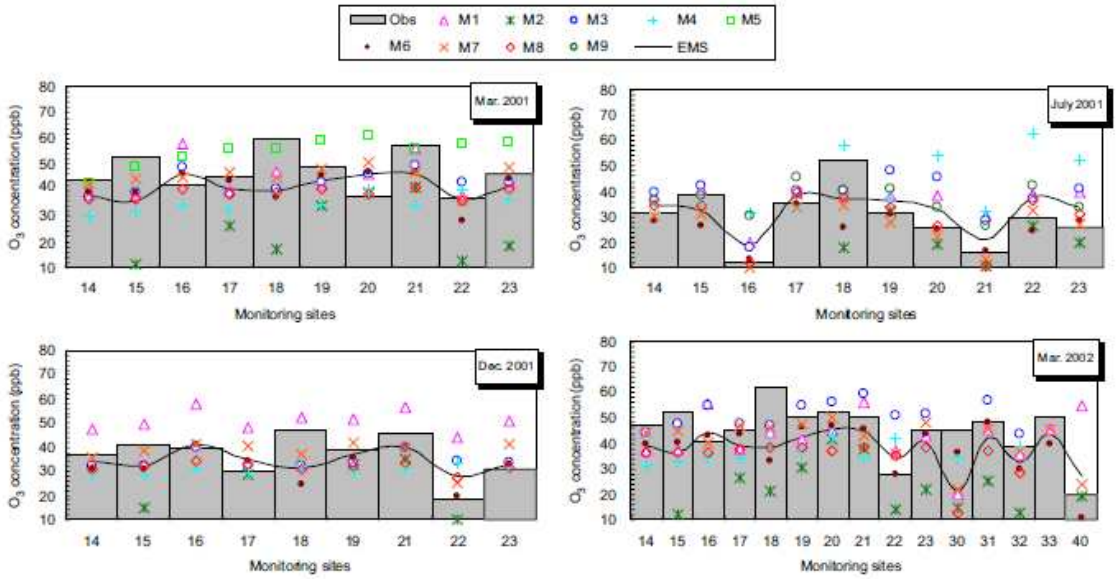

Figure 3.5: Predicted and observed monthly mean near-surface O_3 concentrations. The locations of the observations sites are given in Fig. 3.6. Also shown is the ensemble mean prediction (EMS).

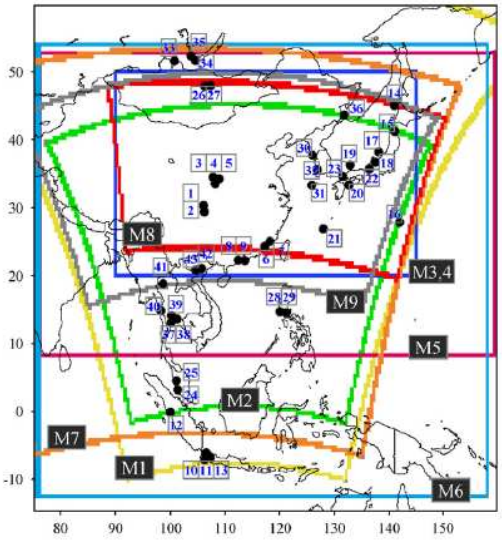

Figure 3.6: The MICS-II study domain. Shown are the domains used by the individual models. Also shown are the EANET observation locations used in the study.

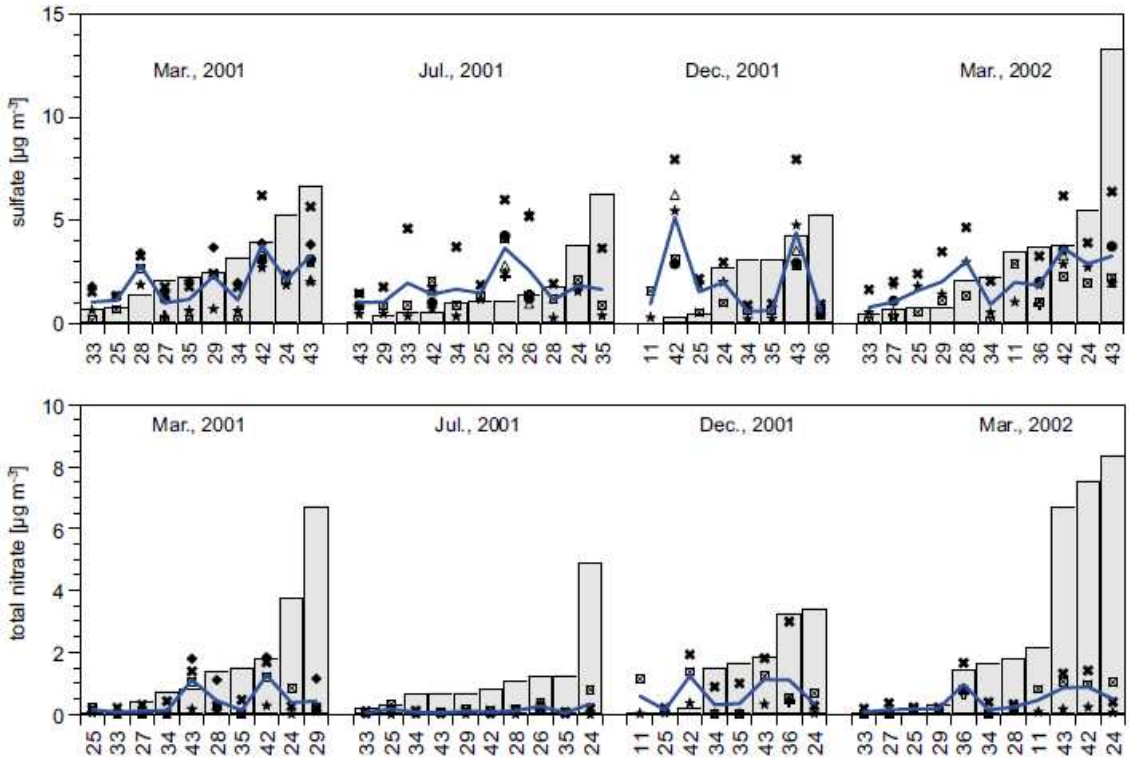

Figure 3.7: Model-observation comparisons with monthly measurements at EANET stations for sulfate and total nitrate.

3.5.2 Over Europe and North America: AQMEII

More than ten state-of-the-art regional air quality models have been applied as part of the Air Quality Model Evaluation International Initiative (AQMEII). These models were run by twenty independent groups in Europe and North America (NA), and standardised modelling outputs over a full year (2006) from each group have been shared [Solazzo *et al.*, 2012b]. The participating models and important characteristics are summarised in Figure 3.8.

For O_3 and PM analyses, Europe and NA are divided into 4 sub-regions for O_3 and 3 for PM. Over Europe, sub-region EU1 consists of the northwestern Atlantic region, France, and northern Spain, and subregion EU2 consists of Central Europe. For O_3 , sub-region EU3 consists of the Po River Valley up to the Alpine area of Italy and southeastern France, and sub-region EU4 covers the Mediterranean area (southern Italy, the east coast of Spain, and Greece). For PM, the sub-region EU3 is included in EU2, and EU3-PM corresponds to EU4-O_3. For NA, for both O_3 and PM analyses, sub-region NA1 consists of the western portion of the United States and southwestern Canada, and sub-region NA3 consists of northeastern NA including parts of south-central Canada. For O_3, sub-region NA2 consists of the U.S. Plains states to the east of the Rocky Mountains, while sub-region NA4 consists of the southeastern United States. For PM, sub-regions NA2 and NA4 are mixed in a sub-region NA2.

As detailed in Solazzo *et al.* [2012b], Figure 3.9 shows time series of the summertime diurnal ozone cycle for (a) EU and (b) NA sub-regions. The majority of individual models (indicated by the thin lines in Figure 3.9) exhibit highly region-dependant behaviour, although some common patterns are present. Models for EU have a predominant tendency to underestimate (in some cases significantly) the peak daily mixing ratio and/or displace the time of the peak mixing ratio, as well as to overestimate nighttime mixing ratios, with the exception of sub-region EU2 (central Europe), which may be due to the strong daily temperature gradient in this region. Nighttime overestimation is known to occur in some models due to difficulties in dealing with stable conditions. Model results for the NA sub-regions exhibit a lower spread throughout the diurnal cycle, with the exception of one outlying model for sub-regions NA1, NA2, and NA3, which is consistently biased low, especially at night. However, the majority of the models exhibited nighttime overestimation to varying degrees, indicating that most of the AQ models have at least some difficulty dealing with stable conditions despite the variety of vertical mixing schemes implemented in the models.

As detailed in Solazzo *et al.* [2012a], Figure 3.10 shows time series of monthly average daily PM_{10} concentrations for the EU and NA domains. A persistent underestimation of PM_{10} by the models is common to both continents and all sub-regions. The models that predict well PM_{10} tend to overestimate $PM_{2.5}$. Figure 3.11 shows time series of monthly average daily $PM_{2.5}$ concentrations for the EU and NA domains. Compared to PM_{10}, model bias is much lower for both continents, demonstrating an enhanced capability of the air quality models to simulate $PM_{2.5}$. The same conclusion was achieved by Roustan *et al.* [2010] who simulated the European air quality during summer and winter 2001 using 30 different model configurations. As shown in Figure 3.12, $PM_{2.5}$ was rather well estimated while PM_{10} was underestimated.

	Model		Res (km)	No. Vertical layers	Emissions	Chemical BC
	Met	AQ				
European Domain	MM5	DEHM	50	29	Global emission databases, EMEP	Satellite measurements
	MM5	Polyphemus	24	9	Standard[a]	Standard
	PARLAM-PS	EMEP	50	20	EMEP model	From ECMWF and forecasts
	WRF	CMAQ	18	34	Standard[a]	Standard
	WRF	WRF/Chem	22.5	36	Standard[a]	Standard
	WRF	WRF/Chem	22.5	36	Standard[a]	Standard
	ECMWF	SILAM	24	9	Standard anthropogenic In-house biogenic	Standard
	MM5	Chimere	25	9	MEGAN, Standard	Standard
	LOTOS	EUROS	25	4	Standard[a]	Standard
	COSMO	Muscat	24	40	Standard[a]	Standard
	MM5	CAMx	15	20	MEGAN, Standard	Standard
North American Domain[b]	GEM	AURAMS	45	28	Standard[c]	Climatology
	WRF	Chimere	36	9	Standard	LMDZ-INCA
	MM5	CAMx	24	15	Standard	LMDZ-INCA
	WRF	CMAQ	12	34	Standard	Standard
	WRF	CAMx	12	26	Standard	Standard
	WRF	Chimere	36	9	Standard	standard
	MM5	DEHM	50	29	global emission databases, EMEP	Satellite measurements

[a] Standard anthropogenic emission and biogenic emission derived from meteorology (temperature and solar radiation) and land use distribution implemented in the meteorological driver (Guenther et al., 1994; Simpson et al., 1995).
[b] Standard inventory for NA includes biogenic emissions (see text).
[c] Standard anthropogenic inventory but independent emissions processing, exclusion of wildfires, and different version of BEIS (v3.09) used.

Figure 3.8: Participating models and important characteristics [Solazzo *et al.*, 2012b].

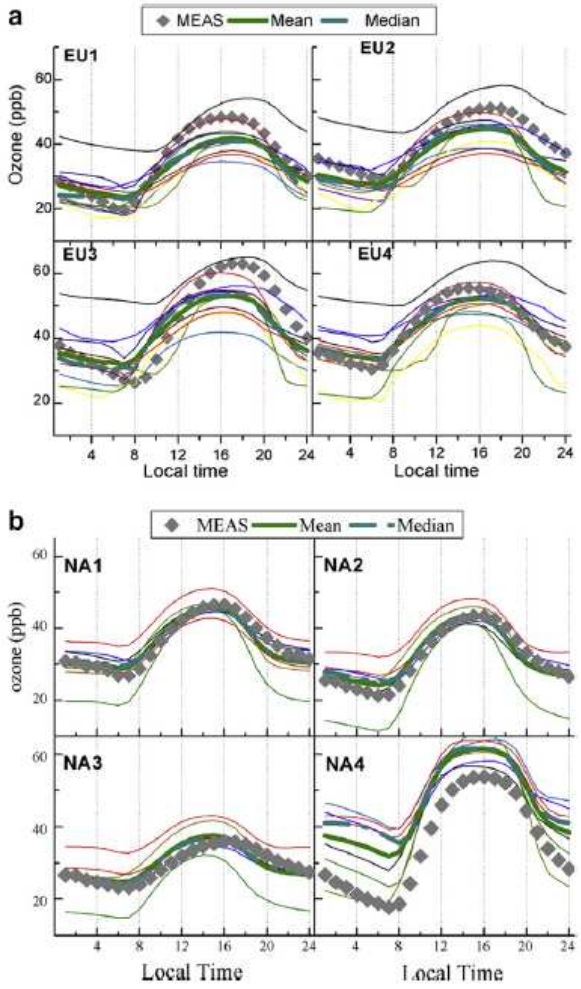

Figure 3.9: Time series of summertime diurnal ozone cycle for (a) EU and (b) NA sub-regions [Solazzo *et al.*, 2012b].

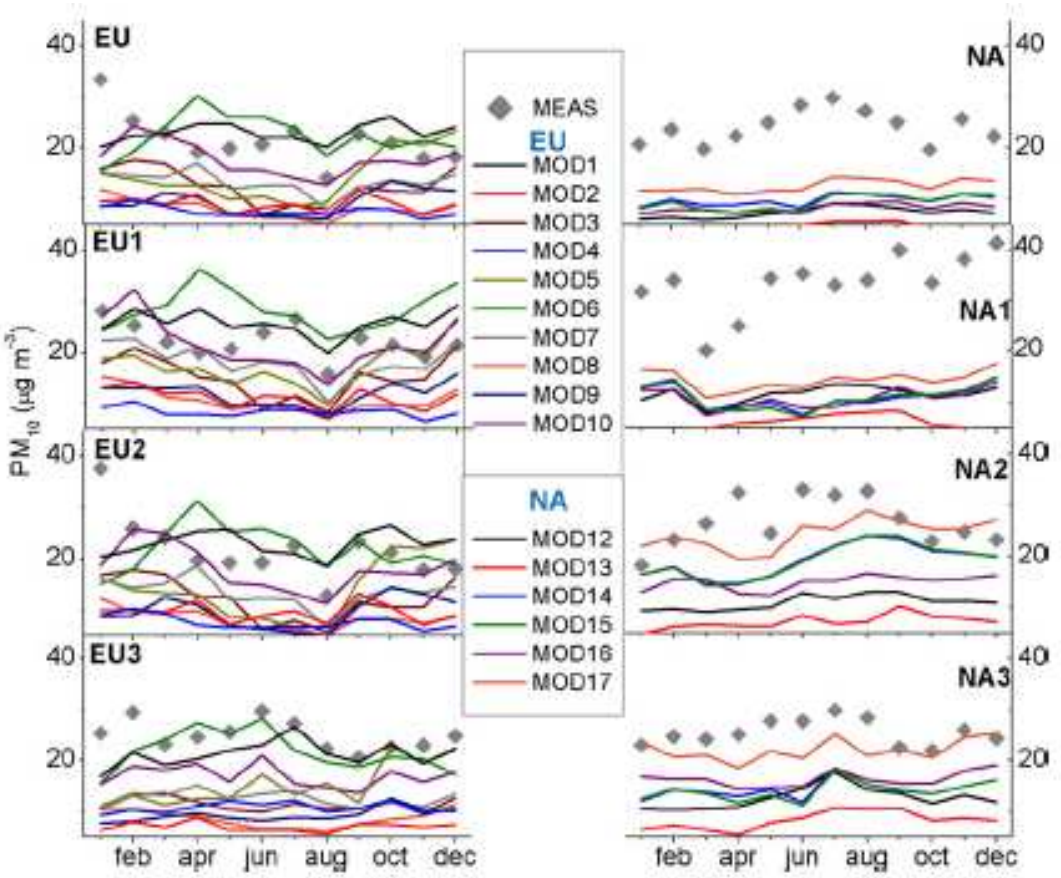

Figure 3.10: Time series of monthly average daily PM_{10} concentrations for the EU (left column) and NA (right column) domains (top row) and sub-regions 1 to 3 (second to fourth rows). Monthly average observed values are represented by the filled diamonds [Solazzo *et al.*, 2012a].

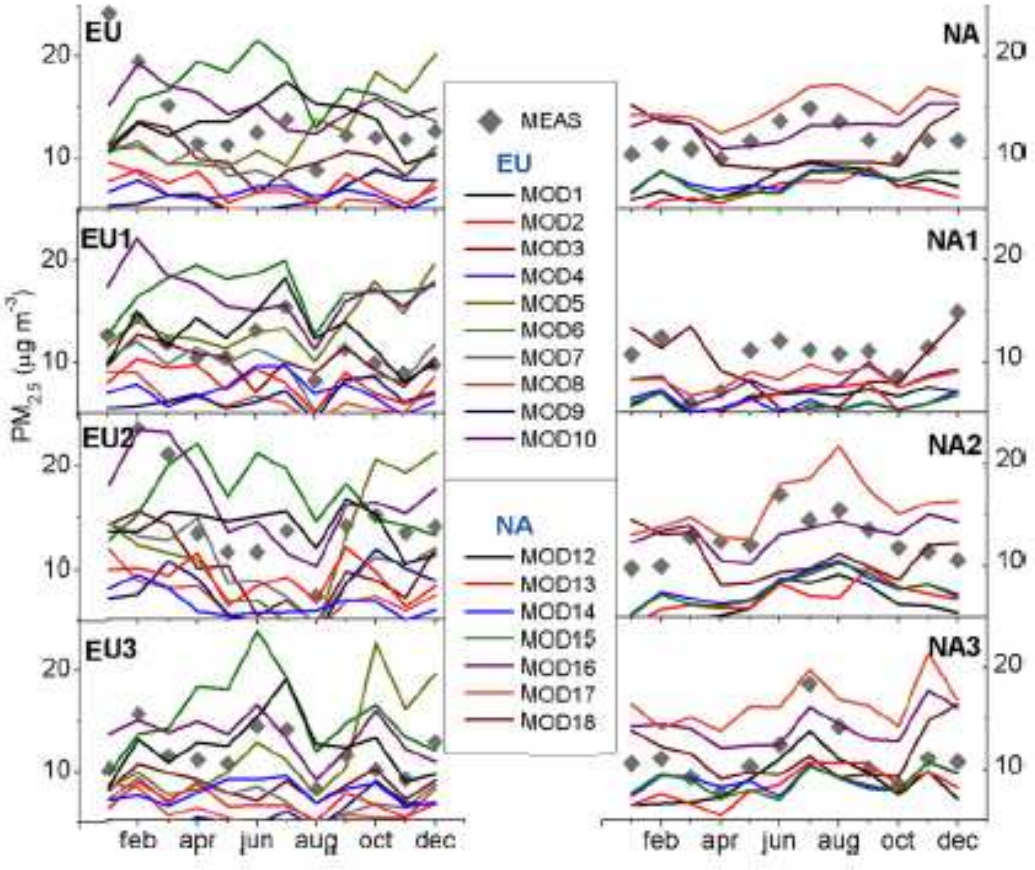

Figure 3.11: Time series of monthly average daily $PM_{2.5}$ concentrations for the EU (left column) and NA (right column) domains (top row) and sub-regions 1 to 3 (second to fourth rows). Monthly average observed values are represented by the filled diamonds [Solazzo *et al.*, 2012a].

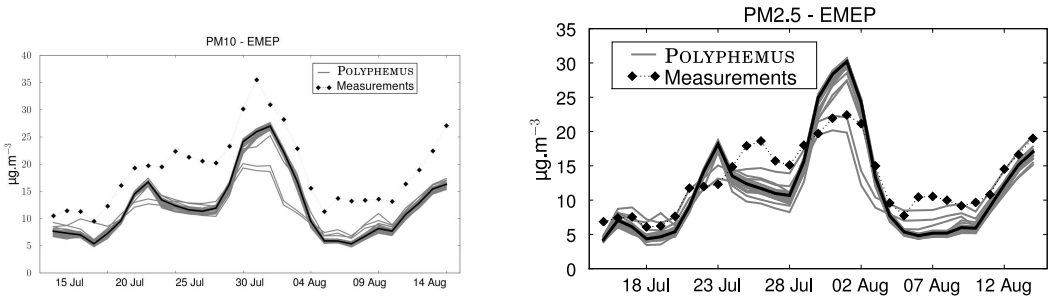

Figure 3.12: Time series of daily concentrations of PM_{10} (left panel) and $PM_{2.5}$ (right panel) averaged over all EMEP stations during the summer period. Each gray line represents results from one model configuration and the black one the reference [Roustan *et al.*, 2010].

Chapter 4

Processes and uncertainties

Air quality predictions are associated to large uncertainties, which originate in

- input data: emissions may be incomplete and/or inaccurate, initial and boundary conditions cannot be accurately defined;
- meteorology and subgrid-scale parameterisations;
- physical and chemical processes which may be parameterised, poorly known and/or even missing;
- numerical approximations.

This chapter first details the conclusions regarding uncertainties that can be drawn from model inter-comparisons: large variations of the concentrations simulated by different models; the variations depend on the chemical components and they are especially large for PM. As uncertainties may be linked to many different processes, it is difficult to understand their origins from model inter-comparisons. Second, the origins of uncertainties are estimated and third, the highest uncertainties for different pollutants are identified from intra-model comparisons.

4.1 Conclusions from model inter-comparisons

Even with similar input data, modelled concentrations obtained from different models greatly differ from each other. In the AQMEII inter-comparisons over North America (NA), most models used the same emission dataset and boundary conditions. However, as shown in Sartelet *et al.* [2012] and in Table 4.1, $PM_{2.5}$ elementary carbon (EC) concentrations greatly vary among models. The mean concentration at observational stations vary by as much as a factor of 5.5 between the model with the lowest concentration and the model with the highest concentration. As EC is an inert component of particles, these variations may be due to meteorology, physical parameterisations such as deposition and numerical approximations. Variations in O_3 concentrations between the models are lower than for PM. The mean concentrations of O_3 at observational stations vary by a factor of 1.3 over NA and 1.6 over Europe, whereas the mean concentrations of $PM_{2.5}$ and PM_{10} vary by factors ranging between 3.8 and 5.7. This suggests that uncertainties in the modelling of PM are higher than in modelling of O_3. Although emissions probably constitute a high source of uncertainties in the modelling (see for example Table 4.2 which shows domain-mean Simpson and MEGAN biogenic emissions used in

AQMEII over Europe by Sartelet *et al.* [2012]), varying the anthropogenic and biogenic emissions leads to variations in O_3 and PM concentrations that are much lower than the variations among the different models.

Because in MICS over East Asia, all models are assumed to use the same input data, the variability between the different models is due to differences in meteorology, physical parameterisations, differences in numerical schemes and differences in the chemical mechanism. To compare the sensitivity of sulfate and nitrate concentrations to the air quality model and to the aerosol module, Sartelet *et al.* [2008] performed runs by switching on and off parameterisations in the aerosol module (intra-model variations). For monthly-averaged concentrations, they found that the variations in sulfate concentrations among the different air quality models are higher than intra-model variations, suggesting that the sensitivity to the aerosol module is weaker than the sensitivity to the air quality model and to the meteorology. However, for nitrate, the variations are of the same order of magnitude, suggesting a very high sensitivity to the aerosol module.

$PM_{2.5}$EC - NA	Polyphemus	AQMEII models		
		Min	Mean	Max
Number of stations	262	262	262	262
Mean obs	0.4	0.4	0.4	0.4
Mean sim	0.5	0.2	0.5	1.1
rmse	0.5	0.5	0.7	1.3
correlation	51.5%	39.5%	46.5%	56.3%
mfb	23.6%	-70.5%	1.5%	80.6%
mfe	56.5%	50.4%	70.7%	90.4%

Table 4.1: Comparisons to observations for surface $PM_{2.5}$ elemental carbon ($PM_{2.5}$EC) over NA for July and August 2006 (concentrations and rmse are in μg m^{-3}). Five models are included in the AQMEII models used for the comparison.

	Simpson	MEGAN
Isoprene	0.0799	0.0312
Terpenes	0.0436	0.01792
Sesquiterpenes	0.000188	0.00129
NO	0.00118	0.00108

Table 4.2: Domain-mean Simpson and MEGAN biogenic emissions (in μg m^{-2} s^{-1}).

4.2 Origins of uncertainties

Uncertainties in pollutant concentrations may have different origins. Although the list below may not be exhaustive, it presents the processes identified as the most important in the modelling of O_3 and PM.

- Initial and boundary conditions; they are usually provided by a larger-scale model and they can not be accurately defined (they are attached to uncertainties of the larger-scale model and to differences in the chemical speciation of the models, which may differ);
- Emissions
  - Estimation of the flux for anthropogenic and natural (biogenic, sea salt, volcanoes, fire) emissions
  - Chemical speciation of emissions
  - Height of release for source anthropogenic emissions, volcanoes and fire emissions
  - Missing sources: e.g. wind-blown dust, road dust resuspension, cooking emissions, semi-volatile organic compounds (SVOC)
- Meteorology
  - Planetary boundary layer scheme and vertical diffusion
  - Land use cover
  - Urban canopy schemes
  - Land surface model
  - Cumulus parameterisation scheme
- Gaseous chemistry
  - Speciation of VOC
  - Aggregation of real species into model species
  - Kinetics of reactions
  - Estimation of photolysis rates
  - Heterogeneous reaction probabilities
  - Oxidation of VOC to SVOC
- Aqueous modelling
  - Aqueous chemistry scheme (especially for organic chemistry)
  - Location of clouds
  - Activation of aerosols in cloud droplets
  - Diameters of droplets
  - Size distribution of aerosols after cloud evaporation

- Aerosol modelling
  - Aerosol dynamics
    - Shape of the size distribution (e.g. modal versus sectional)
    - Numerical approximations to represent the growth by condensation/evaporation (e.g. thermodynamic equilibrium hypothesis between gas and aerosols)
    - Accommodation coefficient for coagulation
    - Parameterisations of the nucleation rate
    - Degree of mixing of particles (internal versus external)
  - Inorganic aerosols
    - Thermodynamic model
    - Limit of the acidity flux
    - Liquid water content
  - Organic aerosols
    - Uncertainties in the enthalpy of vaporisation
    - Ideality assumption for activity coefficients
    - Modelling of anthropogenic SVOC
    - Use of all major secondary organic aerosols (SOA) precursors
    - Modelling of SOA oligomerization
    - Representation of high-NOx and low-NOx gas-phase chemical regimes
    - Hydrophylic vs hydrophobic assumption for chemical components
    - Particle phase reactions leading to further oxidation or fragmentation
    - Heterogeneous oxidation reactions
- Numerical approximations
  - Horizontal and vertical resolutions
  - Number of sections/modes to represent the size distribution of aerosols
- Other processes
  - Dry deposition fluxes: parameterisations on various surfaces, deposition of SVOC
  - Wet deposition fluxes (choice of the diameter of droplets): parameterisations of in-cloud and below-cloud scavenging rates, deposition of SVOC

4.3 Model intra-comparisons

Roustan *et al.* [2010] studied the sensitivity of the ground-level concentrations computed by the air quality model Polair3d/Polyphemus to input data, some parameterisations and numerical approximations. To that end, 30 configurations were derived from a reference configuration of the model by changing one input data set, one parameterisation or one numerical approximation at a time. Each of these configurations was compared to the same reference simulation

over two time periods of the year 2001, one in summer and one in winter. The sensitivity of the model to the different configurations was evaluated through a statistical comparison between the simulation results. The simulations were sorted with respect to the normalised mean error (nme). For all species, the modelled concentrations were very sensitive to the parameterisation used for vertical turbulent diffusion and to the number of vertical levels. For the other configurations considered in this work, the sensitivity of the modelled concentration to the configuration choice varies with the species and the period of the year. Real et Sartelet [2011] studied for the same two time periods of the year 2001 as Roustan *et al.* [2010] the sensitivity of the modelled concentrations to the modelling of photolysis rates (cloud parameterisation and aerosols). Kim *et al.* [2009, 2011b] compared two recent gas-phase chemical kinetic mechanisms (CB05 and RACM2) for the formation of ground-level ozone over Europe, and for the formation of secondary inorganic and organic aerosols during the summer time period of the year 2001 modelled by Roustan *et al.* [2010]. For the same time period, Kim *et al.* [2011a] compared the effects of the two gas-phase chemical kinetic mechanisms (CB05 and RACM2) and two SOA modules, the Secondary Organic Aerosol Model (SORGAM) and AER/EPRI/-Caltech model (AEC), on $PM_{2.5}$ formation.

4.3.1 Ozone

Roustan *et al.* [2010] and Real et Sartelet [2011] found that O_3 is mainly sensitive to the parameterisation used for vertical diffusion (turbulence parameterisation) with an nme of 14% in summer and 18% in winter, the number of model levels with an nme of 8% in summer and 12% in winter, the input data used for boundary conditions with nme between 7 and 8% in summer and between 4 and 6% in winter, the inclusion of aerosols when computing photolysis rates with a nme of 4% in summer and 2% in winter, and the heterogeneous reaction probabilities with nme between 2% and 3%. The large impact of the vertical diffusion on the modelled O_3 concentrations confirms the results presented by Mallet et Sportisse [2006]. Between the first two layers, the vertical diffusion coefficient values obtained with the Louis parameterisation are lower than those of the Troen and Mahrt parameterisation. The mass exchange between the first layer and the second one, richer in ozone, is then decreased. That explains the negative bias and the lower value of the mean concentration.

Kim *et al.* [2009] compared CB05 and RACM2 for simulations of ozone over Europe. Changing the gas-phase chemical kinetic mechanisms from CB05 to RACM2 leads to a nme of 5% in summer. Significant differences, however, appear at specific locations. Figure 4.1 shows monthly averages of daily maximum 8h-average ozone concentrations (ppb) modelled with CB05 and RACM2, and differences between the two model simulations by modulus. This difference results from different treatments in the two mechanisms for both inorganic and organic chemistry. Differences in the treatment of the inorganic chemistry are due mainly to differences in the kinetics of two reactions: $NO + O_3 \rightarrow NO_2 + O_2$ and $NO + HO_2 \rightarrow NO_2 + OH$. These differences lead to a domain-averaged difference in ozone concentration of 5%, with RACM2 kinetics being more conducive to ozone formation. Differences in the treatment of organic chemistry lead to a domain-averaged difference in ozone concentration of 3%, with CB05 chemistry being more conducive to ozone formation.

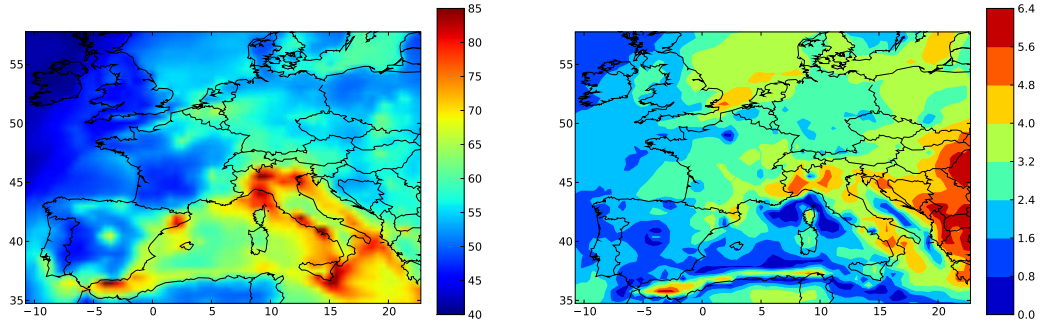

Figure 4.1: Monthly average of daily maximum 8h-average ozone concentrations (ppb) modelled with CB05 (left column), and differences between the two model simulations by modulus (right column) [Kim *et al.*, 2009].

4.3.2 PM_{coarse}

As detailed by Roustan *et al.* [2010], although PM_{coarse}, which is the difference between PM_{10} and $PM_{2.5}$, is influenced by many aerosol parameterisations, it is systematically underestimated in summer and winter. This underestimation may be partly explained by the treatment applied to boundary conditions to deal with Saharan dust episodes which are partly neglected [Sartelet *et al.*, 2007a] and by the lack of natural dust emissions and road resuspension in the emissions inventory.

PM_{coarse} is very sensitive to the parameterisation used for sea-salt emission, with nme between 53-59%, the vertical diffusion with nme between 28-46%, the number of levels with nme between 21-24%, to the mixing of sea-salt particles with pollution particles with nme between 20-24%, to options related to deposition (e.g. computation of wet diameter) with nme between 9 to 19%, to assumptions in computing mass transfer rates between gas and aerosols with nme between 15 and 19%, to boundary conditions with a nme of 6% algorithms and to redistribution algorithms after aqueous chemistry with a nme of 6%.

4.3.3 $PM_{2.5}$

Roustan *et al.* [2010] showed that modelled concentrations of $PM_{2.5}$ are sensitive to a larger number of configurations than PM_{coarse}.

$PM_{2.5}$ concentrations are highly sensitive to the parameterisation used for vertical diffusion with nme between 19 and 23%, to options related to sea-salt aerosols with nme between 12 and 23%, to boundary conditions with nme between 9 and 30%, to the number of vertical levels used with nme between 11 to 16%, to heterogeneous reactions with nme between 3 to 21%, to assumptions in computing mass transfer rates between gas and aerosols with nme between 8 and 12%, to the criterion selected to activate aqueous chemistry with nme between 8 and 13%, to options related to deposition (e.g. computation of wet diameter) with nme between 4 to 9%. Choices of the size distribution and the aerosol density have both an nme of 6%.

For the summer simulation, the nme is 8% if the gas-phase chemical kinetic mechanism

is changed from CB05 to RACM2. As shown by Kim *et al.* [2011b], this difference is due to inorganic aerosols (sulfate, ammonium and nitrate) and organic aerosols (biogenic and anthropogenic). Differences may be higher for specific compounds (nitrate, organic compounds). Differences in the inorganic and organic aerosols result primarily from differences in oxidant concentrations (OH, O_3 and NO_3). For example, the nme for OH and NO_3 is as high as 36% and 22%, respectively.

The impact of taking into account aerosols when computing photolysis rates is lower and the nme is only 3% in the summer for $PM_{2.5}$, with difference in OH concentration as high as 15% [Real et Sartelet, 2011].

4.3.4 Sulfate

Sulfate concentrations are very sensitive to the boundary conditions with nme between 6 and 31%, to the vertical diffusion and to changes of the number of levels with nme between 10 to 17%, to the criterion selected to activate aqueous chemistry and to the aqueous chemistry with nme between 9 and 14%, to heterogeneous reactions with nme between 9 and 11%, to deposition (e.g. computation of wet diameter) with nme of 6%, and the dynamical treatment of the gas-particle mass transfer with an nme of 5%.

When changing the gas-phase chemical kinetic mechanism from CB05 to RACM2, during the summer period, the nme is as high as 16% for sulfate because of high differences in OH concentrations.

4.3.5 Nitrate

Nitrate concentrations show a high variability depending on the options used in the air quality model (AQM), with higher nme than other pollutants. Nitrate concentrations are very sensitive to vertical diffusion and to changes of the number of levels with nme between 25 and 33%, to whether Na^+ and Cl^- are treated in the thermodynamic module or not (i.e. mixing of aerosols) with nme between 70 and 90%, to heterogeneous reactions with nme from 22 to 65%, to the thermodynamic model used with nme between 7% in winter and 41% in summer, to the dynamical treatment of the gas-particles mass transfer with nme between 16 and 26%, to the aqueous chemistry model with nme between 19 and 23%, to the criterion used to call the aqueous chemistry model with nme between 11 and 16%, to the dry deposition of the gaseous precursor HNO_3 with nme between 7 and 11%, to deposition (e.g. computation of wet diameter) with nme between 7 and 8% .

When changing the gas-phase chemical kinetic mechanism from CB05 to RACM2, during the summer period, the nme is as high as 19% for nitrate because of differences in the concentrations of HNO_3 (nme of 28%) where the concentrations of ammonia are high.

4.3.6 Ammonium

Ammonium concentrations show variabilities depending on the options used in the AQM higher than sulfate but lower than nitrate. Ammonium concentrations are very sensitive to vertical diffusion and to changes of the number of levels with nme between 13 and 24%, to heterogeneous reactions with nme from 7 to 37%, to whether Na^+ and Cl^- are treated in the thermodynamic

module or not (i.e. mixing of aerosols) with nme between 20 and 23%, to the aqueous chemistry model used with nme between 11 and 21%, to the criterion used to call the aqueous chemistry model with nme between 9 and 11%, to the dynamical treatment of the gas-particles mass transfer with nme between 13 and 16%, to the thermodynamic model used with a nme of 12% in summer, to the algorithm used for mass redistribution after condensation/evaporation with a nme of 8% in winter, to deposition (e.g. computation of wet diameter) with a nme of 5%.

When changing the gas-phase chemical kinetic mechanism from CB05 to RACM2, during the summer period, the nme is as high as 14% for ammonium because of differences in the concentrations of sulfate and ammonium.

4.3.7 Organic matter

Roustan *et al.* [2010] did not include SOA nor organic matter (OM) in their sensitivity study. Kim *et al.* [2011b] compared CB05 and RACM2 for simulations of PM including SOA for the summer period of 2001. Differences in organic aerosols result mostly from differences in oxidant concentrations (OH, O_3 and NO_3). The difference in monthly-mean concentrations of anthropogenic SOA is 22%, which corresponds to a nme of 20%. Most of that difference is due to aromatic SOA. Differences in the contribution of aromatics to anthropogenic aerosol formation are due to the fact that aromatics oxidation in CB05 leads to more cresol formation from toluene oxidation. Differences in the aromatic aerosols would be significantly reduced with the recent CB05-TU mechanism for toluene oxidation. The difference in monthly-mean concentrations of biogenic SOA is 1%, which corresponds to a nme of 5%. The difference is low because of compensating differences of higher concentrations of the monoterpene oxidation product BiBmP with CB05 (+12%) and lower concentrations of the other biogenic SOA (-4%). Differences in the biogenic aerosol formation are partly due to differences in oxidant concentrations and partly to the total organic mass, which influences the formation of biogenic aerosol by gas-particle partitioning coefficients. The maximum local differences of aerosol formed from monoterpene SVOC are 12% (BiA0D), 52% (BiA1D), 45% (BiA2D) and 91% (BiBmP). For the aerosol formed from isoprene SVOC, the maximum local differences are 21% (BiISO1) and 16% (BiISO2).

For the summer period of 2001, Kim *et al.* [2011a] compared the effects of the two gas-phase chemical kinetic mechanisms RACM2 and CB05 and the two SOA modules SORGAM and AEC, on fine $PM_{2.5}$ formation. The major sources of uncertainty in the chemistry of SOA formation were investigated. The use of all major SOA precursors and the treatment of SOA oligomerization were found to be the most important factors for SOA formation, leading to 66% and 60% more SOA, respectively. The nme between simulations with and without biogenic SOA precursors (isoprene and sesquiterpenes) is as high as 70% with SORGAM. The nme between simulations with and without oligomerization in the SOA model AEC is 24%. For August 2002, Couvidat *et al.* [2012a] found a nme of the same order of magnitude, 36%, between simulations with and without oligomerization in the SOA model H^2O. Kim *et al.* [2011a] also found that the explicit representation of high-NOx and low-NOx gas-phase chemical regimes may also lead to an important increase of SOA depending on the approach used to implement the distinct SOA yields within the gas-phase chemical kinetic mechanism; Implementing the high-NOx and low-NOx SOA yields not in the first oxidation step of the precursor species for aromatics but in later oxidation steps corresponding to reactions of precursor oxidation prod-

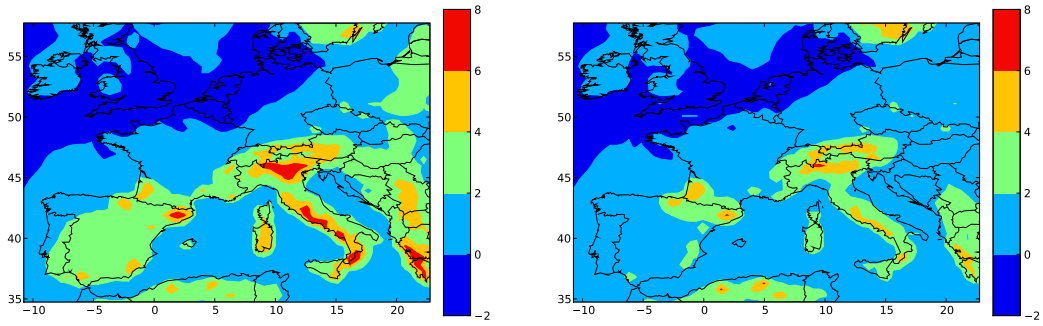

Figure 4.2: Differences in $PM_{2.5}$ concentrations (μg m^{-3}) over Europe simulated with RACM2 and CB05 for gas-phase chemistry and with AEC and SORGAM for SOA formation. Results are averaged over the one-month simulation of 15 July to 15 August 2001: $[PM2.5]_{CB05,AEC}$ - $[PM2.5]_{CB05,SORGAM}$ (left column); $[PM2.5]_{RACM2,AEC}$ - $[PM2.5]_{RACM2,SORGAM}$ (right column) [Kim *et al.*, 2011a]

ucts with nitrogenous species and peroxyl radicals leads to a nme of 34% using SORGAM. The treatment of isoprene SOA as hydrophobic or hydrophilic leads to a significant difference, with more SOA being formed in the latter case, and a nme of 6% for August 2002 with H^2O(Couvidat *et al.* [2012a]). The activity coefficients may also be a major source of uncertainty, as they may differ significantly between atmospheric particles, which contain a myriad of SOA, primary organic aerosol (POA), and inorganic aerosol species, and particles formed in a smog chamber from a single precursor under dry conditions. Assuming ideality (i.e., the activity coefficients are equal to one) leads to a nme of 11% with H^2O in August 2002. The values of the enthalpies of vaporization for the equilibrium calculations of hydrophobic SOA have been shown to have some effects on average SOA concentrations. Kim *et al.* [2011a] replaced the original enthalpies of vaporization of SORGAM (156 kJ/mol for all SOA) by a value of 88 kJ/mol, which better reflects the more recent estimated values. The difference in SOA concentrations averaged over the entire domain is low (0.01 μg m^{-3}), but corresponds to a nme of 14%. Couvidat *et al.* [2012a] found that taking into account the gas-phase fraction of SVOC increases significantly organic PM concentrations, especially during winter, with a nme of 59% on SOA concentrations for February 2003.

Finally, significant interactions exist between the uncertainties of the gas-phase chemistry and those of the SOA module. For example, Figure 4.2 shows differences in $PM_{2.5}$ concentrations (mug m^{-3}) simulated with AEC and SORGAM for SOA formation and either RACM2 or CB05 for gas-phase chemistry. The effect of the aerosol module differs depending on which gas-phase chemical mechanism is used.

4.4 Discussion

The choice of the parameterization for the vertical turbulent diffusion coefficient and the choice of the vertical levels, have a large impact on the modeled concentrations at the surface of all

the considered species. The options related to boundary conditions have a large impact on the species that have a long lifetime and are treated with explicit fields derived from global models (O_3, NO_2, sulfate and ammonium).

The formulation of a gas-phase chemical kinetic mechanism for ozone can have significant direct (e.g., cresol formation) and indirect (e.g., oxidant levels) effects on PM formation. Furthermore, the incorporation of SOA into an existing gas-phase chemical kinetic mechanism requires the addition of reactions and product species, which should be conducted carefully to preserve the original mechanism design and reflect current knowledge of SOA formation processes (e.g., NOx dependence of some SOA yields). The development of chemical kinetic mechanisms, which offer sufficient detail for both oxidant and SOA formation is recommended.

The current state of the science is more advanced for the gas-phase chemistry of ozone formation than for the chemistry and gas/particle partitioning of particulate matter (PM) formation. As a result, there are larger uncertainties associated with aerosol modules than with gas-phase chemical kinetic mechanisms. Nevertheless, the uncertainties associated with those modules are not additive in an air quality model and there are close interactions between the gas phase chemical mechanism and the secondary aerosol formation. In particular, the effect of the NOx regime on SOA formation should be explicitly treated in air quality models.

Chapter 5

Perspectives

Aerosol modelling has strongly improved over the past fifteen years. The modelling of inorganic chemical compounds are now relatively well understood, although some reactions still need to be better constrained, as discussed in Chapter 4. Further work will be devoted to improve the modelling of secondary organic aerosols (SOA), to better model some of the aerosol properties, such as mixing properties, the number concentrations of particles, and to better characterise primary emissions, such as the ration primary organic aerosols (POA) over semi-volatile organic compounds (SVOC). Model evaluation of the aerosol properties and concentrations is also important to assess the performance of the models and to help directing the improvements that need to be made.

5.1 Mixing properties of aerosols

Air quality models (AQM), such as the one integrated in the air-quality platform Polyphemus, allow us to simulate pollutant concentrations from emission inventories, meteorological data and the boundary conditions of the domain studied. In those models, particles of a given diameter are assumed to mix instantaneously when they meet because of transport, such as advection by wind. This hypothesis is called "internal mixing hypothesis". Although particles do mix progressively under the effects of coagulation, and condensation/evaporation, this hypothesis may be difficult to justify close to emission sources. Many observations, such as those of Healy *et al.* [2012] in Paris, suggest that particles from different sources are often not mixed. The internal mixing assumption allows one to lower computational cost for air-quality modelling. Taking into account particles that are externally mixed in a model increases the memory space required by the program to run, as well as the computing time.

The mixing state of particles strongly influences optical properties and the formation of particles by influencing the chemical composition. For the formation of SOA, mixing influences the hydrophilic and organic absorbing properties of particles. A new PM module, which represents the mixing state of particles by discretising the aerosol composition (the fraction of families of chemical components) as well as the size distribution, is currently being developed. The method developed here allows one to model the mixing dynamics: particles are not either mixed or unmixed, but they can be partially mixed as represented by the mass fraction of particle chemical components. So far, the model represents the coagulation of particles [Dergaoui *et al.*, 2013], see Section 2.5. When two particles of different compositions coagulate, the resulting particle has a composition that is different from those of the two particles that

have coagulated. The model needs to be generalised to model condensation/evaporation and to be integrated in a 3D AQM. Under condensation/evaporation, particle diameter grows/shrinks. For 3D applications, the sections need to be of distinct size ranges throughout the simulations. As particles grow/shrink with condensation/evaporation, the bounds of the sections and the particle diameter evolve, as seen in Chapter 2, and it is then necessary to redistribute the number and mass among the fixed size sections. Similarly, the chemical compositions of particles evolve, and an algorithm will be developed to redistribute the particles amongst the different mass-fraction sections. The externally mixed aerosol model will then be integrated in the air-quality platform Polyphemus and coupled to the Polair3D/Polyphemus AQM.

Comparisons of the mixing-state of particles using Polyphemus with the newly developed externally mixed aerosol model to measurements will be conducted over Greater Paris. During the winter 2010 MEGAPOLI (Megacities: Emissions, urban, regional and Global Atmospheric POLlution and climate effects, and Integrated tools for assessment and mitigation) campaign, using an Aerosol Time-Of-Flight Mass Spectrometer (ATOFMS), Healy *et al.* [2012] found that biomass burning particles from local domestic wood burning sources are not mixed to low-diameter traffic particles, which could also be differentiated from higher diameters internally-mixed particles with inorganic compounds (majoritarily either sulfate or nitrate compounds). By allowing different mass fractions of chemical compounds for a given particle size, the new model will allow us to better quantify the impact of regional versus local sources.

The development of the externally mixed aerosol model and comparisons to measurements over Greater Paris will be done in the framework of the Ph.D. thesis of Shupeng Zhu. Further measurements of the mixing properties of particles will be made during the ChArMEx (Chemistry-Aerosol Mediterranean Experiment) campaign in summer 2013 in the framework of the ANR SAF-MED (Secondary Aerosol Formation in the MEDiterranean).

5.2 Secondary Organic Aerosols

5.2.1 Chemical gas-phase mechanisms

Understanding the formation of SOA is complicated because of difficulties to correctly characterise the gas-phase oxidant chemistry and the multi-step oxidation of volatile organic compounds (VOC) that lead to SOA formation. Most state-of-the-art AQM may actually not be valid far from source regions because SOA formation in AQM is based only on the first and, in some cases, second VOC oxidation steps.

The chemical gaseous schemes currently used were mostly designed to correctly model ozone concentrations, and they are lacking details on the oxidation of VOC that may form semi-volatile organic compounds (SVOC), which can then condense onto particles. The incorporation of SOA into an existing gas-phase chemical kinetic mechanism requires the addition of reactions and product species, which should be conducted carefully to preserve the original mechanism design and reflect current knowledge of SOA formation processes (e.g., NO_x dependence of some SOA yields). Most of the existing SOA chemical mechanisms are based on chamber experiments. These measurements do not derive patterns with several chemical steps of oxidation of organic compounds, and it is often not possible to identify all the organic compounds produced by oxidation. But it is now recognised that it is crucial to take into account several oxidation steps to properly represent the formation of SOA. Explicit chemical schemes, such as GECKO [Camredon *et al.*, 2007], have been developed to take into account the different

stages of oxidation, but they are too costly in calculation time to be used in 3D. Using available kinetic and thermodynamic data and structure-reactivity relationships, they typically include several hundred thousand organic species and up to a million reactions. However, they could be used as a benchmark to develop parameterisations of third and fourth generation oxidation products.

5.2.2 Multiphase models

The formation of organic aerosols is a complex phenomenon involving many processes (absorption in an organic or aqueous phases, oligomerization, hygroscopicity). Organic aerosol models like AEC or H^2O take into account the influence of the non-ideality of aerosols and distinguish hydrophilic (which condense on an aqueous phase) and hydrophobic (which condense on an organic phase) compounds. However, this type of model could be improved by allowing some compounds to condense both on an organic phase and an aqueous phase. Simulations show that some compounds from the oxidation of monoterpenes can be both hydrophilic and hydrophobic while some compounds from oxidation of isoprene are very hydrophilic. Furthermore, this type of model does not take into account the possible influence of saturation of the organic phase. A study of the MEGAPOLI summer campaign [Couvidat *et al.*, 2012b] suggests that the primary compounds and secondary compounds do not easily mix. It is therefore desirable to be able to take into account the saturation of the organic phase and the co-existence of two or more distinct organic phases. The model could also be improved by taking into account the viscosity of particles, which could strongly influence the equilibrium between gas and particle and, therefore, affect the partitioning between the gas and the particle phases. The development of such a model will be made in the framework of the post-doctorat of Florian Couvidat for the GMES-MDD project "Amélioration des émissions naturelles et de la chimie organique des aérosols pour la prévision de chimie-transport sur l'Europe."

5.3 Modelling number concentrations

As several epidemiological studies have suggested statistical relationships between adverse health effects and fine and ultrafine particles, it is crucial to not only evaluate models for the modelling of mass concentration but also for number. Modelling the number concentration is important not only for fine particles, but also for larger particles that can act as cloud condensation nuclei, as they control the aerosol-cloud interactions and affect the climate [Lohmann et Feichter, 2005].

High mass concentrations are mostly observed for coarse and fine particles, while high number concentrations are mostly observed for ultrafine particles. The modelling of ultrafine particles is more difficult than fine and coarse particles, because processes such as nucleation, Kelvin effect and Van der Walls forces may become important. Current modal models have shown to not be inadequate to model the growth of ultrafine particles.

Recently, simultaneous measurements of number concentrations at different stations have been performed, e.g. during the MEGAPOLI campaign over Paris and over Europe as part of the ACTRIS (Aerosols, Clouds, and Trace gases Research InfraStructure Network) project. An evaluation of models using recent measurements is therefore desirable and is currently under progress for the MEGAPOLI campaign in the framework of the Ph.D. thesis of Stephanie

Deschamps.

5.4 Model evaluations

A better description of PM concentrations and characteristics (particle size distribution, chemical composition, volatility, hygroscopicity and mixing state) from both measurements and modelling is desirable to improve our understanding of the origins, evolution, and properties of organic aerosols (OA).

High secondary organic aerosols (SOA) concentrations have been observed in summer over the Mediterranean basin, where high natural emissions (biogenic and oceanic) are common and where aged anthropogenic plumes are transported. The ANR SAF-MED, which started in November 2012, aims to develop a better understanding of the origins of the high SOA concentrations observed in the western Mediterranean in summer with a focus on the role of atmospheric chemical processing and particle properties in SOA formation, in the framework of ChArMEx (The Chemistry-Aerosol Mediterranean Experiment, http://charmex.lsce.ipsl.fr). The general strategy aims to document the chemical processing of air masses of different origins and at various times since their emission. This will be addressed by combining full-chemistry ground-based measurements at one receptor site and pseudo-Lagrangian airborne measurements following an air parcel for a few days. A four-week intensive field measurement campaign will be performed at a receptor site at Ersa on the northern coast of Corsica (wind turbine site, ChArMEx supersite), between mid-July 2013 and mid-August 2013. The ERSA super-site appears to be the most suitable location to investigate the role of atmospheric aging on OA concentration levels and properties, as it benefits from a high level of photochemical activity during summertime. Furthermore, although not strongly influenced by local anthropogenic sources, the ERSA site is often impacted by air masses originating from both the Po Valley and Rhone Valley reacting over the Mediterranean and/or the Ligurian Sea, thus by air masses more distant from sources as those encountered during the Megapoli campaign in Paris. A better characterisation of SOA and PM will allow us to evaluate existing AQM. Not only PM concentrations, but also PM properties will be compared to measurements, leading to stronger constraints on AQM. As a large part of SOA may be formed from the interactions between biogenic and anthropogenic precursors, improvements in the modelling of natural and anthropogenic aerosols will allow us to better quantify the part of biogenic SOA that can be controlled.

5.5 Primary emissions

Primary emissions are either anthropogenic or natural. Natural emissions are related to aerosol dust minerals, forest fires, sea salt and biogenic emissions. They are still attached to high levels of uncertainties.

5.5.1 Anthropogenic emissions

Anthropogenic emissions are provided by emission inventories, which detail the emissions of different pollutants (typically VOC, NO_x, CO, SO_2, $PM_{2.5}$, PM_{10}, CH_4) for different activity sectors. The inventory species are disaggregated into real species using speciation coefficients.

For example, NO_x emissions are split into NO and NO_2; for VOC over Europe we use the speciation of Passant [2002]. PM are split amongst different chemical species (usually organic, elemental carbon and dust), and number concentration is usually not estimated.

5.5.1.1 Organics

Primary organic aerosols (POA) are in fact condensed semi-volatile organic compounds (SVOC), which exist in both the gas phase and the particle phase. Although SVOC present in the particle phase are considered in emission inventories, those in the gas-phase are not, because they are often made of species of more than 12 carbons, which are usually not measured. For traffic emissions, inventories are built by measuring the concentration of POA after some dilution. This POA concentration varies depending on the dilution, the temperature, as SVOC may evaporate from the particle phase. Typically, for diesel traffic emissions, as shown by Robinson *et al.* [2007], if POA measurements are performed at ambient concentrations (a few μg m^{-3}), then the gaseous fraction of SVOC could be estimated using a ratio SVOC/POA ratio of 5. This ratio is highly uncertain, as only few measurements have been performed at ambient concentrations, and it needs to be estimated for different vehicle categories, as planned in the project DRIVE (Emissions particulaires Directes et Indirectes du trafic routier) coordinated by Aurélie Charron from IFSTTAR, in which we participate. Measurements for other emission inventory categories are also required.

5.5.1.2 Number

Number concentration is not yet provided by anthropogenic emission inventories which only provide mass. The size distribution of ultrafine particles are usually not known, as inventories only provide PM or $PM_{2.5}$ and PM_{10} concentrations. However, in the tool COPERT 4 used to calculate air pollutant and greenhouse gas emissions from road transport, emission factors for particle number are estimated. These factors, and factors estimated in the framework of the project PM-DRIVE, should be used to estimate number emissions from emission inventories.

5.5.2 Natural emissions

Natural particle emissions are still attached to high level of uncertainties. They are related to mineral aerosols, fire and sea salt. Their relative contribution to overall emissions is highly dependent on the period of the year and highly variable spatially. The modelling of these emissions will be improved in the framework of the GMES-MDD project “Amélioration des émissions naturelles et de la chimie organique des aérosols pour la prévision de chimie-transport sur l’Europe.”

5.5.2.1 Sea-salt

Marine emissions emit mainly chlorine, sodium (and a few other inorganic species such as sulfate) and organics. Most existing parameterisations in AQMs represent only the inorganic emissions. It is only recently that parameterisations have been developed to model the primary marine organic emissions [Gantt *et al.,* 2011]. The organic aerosol is due to marine phytoplankton, which emits different volatile organic compounds that can form particles (isoprene,

terpenes) but also primary organic particles. These emissions will be estimated using the parameterisation of Gantt *et al.* [2011], and satellite data giving the location and the concentration of the phytoplankton.

5.5.2.2 Dust

Sahara mineral dust can be transported over long distances, e.g. from Sahara in Africa to Europe. Emission models depend on the wind speed and parameters such as roughness, mineralogy and surface type. The high variabilities of Sahara dust events make it difficult to forecast. In the forecast made with the air-quality platform Polyphemus (http://cerea.enpc.fr/en/prevision.html), European boundary conditions are obtained from global simulations averaged over several years. The variabilities of Sahara dust events cannot therefore be reproduced. In the framework of the GMES-MDD project, the tools developed at the Laboratoire de Météorologie Dynamique (LMD) to model Saharan dust will be shared to improve the modelling of mineral aerosol concentrations over Europe.

5.5.2.3 Fire

For biomass burning emissions, emission inventories are built from satellite observations of active fires and burned areas, e.g. by Solène Turquety in the framework of the project API-FLAME, in which we participate. Emissions can be injected into the boundary layer or above and these highly uncertain injection heights may strongly affect the ground-level concentrations, as shown in Couvidat *et al.* [2012a]. In the framework of the GMES-MDD project, the speciation of the inventory of Solène Turquety will be modified to take into account the species developed in the organic aerosol model developed in the project.

5.5.3 Resuspension of road dust

$PM_{2.5}$ are now quite well modelled. However, PM_{10} concentrations are still often underestimated. This under-estimation may be a consequence of several processes that are not taken into account in most models, such as resuspension of road dust by vehicular traffic and/or particulate emissions from car brakes. As new data become available, parameterisations may be developed to include those emissions in air-quality models.

Appendix 1: Evolution equations of moments by coagulation

If 3 modes are considered, the evolution equations of moments by coagulation may be written for each mode i, j and k as

$$\begin{aligned}
\left(\frac{\partial M_{0_i}}{\partial t}\right)_{coag} &= 0.5\ I_{i,i}^{0,0} - I_{i,j}^{0,0} - I_{i,k}^{0,0} \\
\left(\frac{\partial M_{0_j}}{\partial t}\right)_{coag} &= 0.5\ I_{j,j}^{0,0} - I_{j,k}^{0,0} \\
\left(\frac{\partial M_{0_k}}{\partial t}\right)_{coag} &= 0.5\ I_{k,k}^{0,0} \\
\left(\frac{\partial M_{3_i}^{cs}}{\partial t}\right)_{coag} &= -F_i^{cs}\ I_{i,j}^{3,0} - F_i^{cs}\ I_{i,k}^{3,0} \\
\left(\frac{\partial M_{3_j}^{cs}}{\partial t}\right)_{coag} &= F_i^{cs}\ I_{i,j}^{3,0} - F_j^{cs}\ I_{j,k}^{3,0} \\
\left(\frac{\partial M_{3_k}^{cs}}{\partial t}\right)_{coag} &= F_i^{cs}\ I_{i,k}^{3,0} + F_j^{cs}\ I_{j,k}^{3,0} \\
\left(\frac{\partial M_{6_i}}{\partial t}\right)_{coag} &= I_{i,i}^{3,3} - I_{i,j}^{6,0} - I_{i,k}^{6,0} \\
\left(\frac{\partial M_{6_j}}{\partial t}\right)_{coag} &= I_{i,j}^{6,0} + I_{j,j}^{3,3} + 2\ I_{i,j}^{3,3} - I_{j,k}^{6,0} \\
\left(\frac{\partial M_{6_k}}{\partial t}\right)_{coag} &= I_{i,k}^{6,0} + I_{j,k}^{6,0} + 2\ I_{i,k}^{3,3} + 2\ I_{j,k}^{3,3} + I_{k,k}^{3,3}
\end{aligned} \tag{5.1}$$

where cs denotes the chemical species, F_l^{cs} denotes the volume proportion of chemical species in mode l ($l = i, j, k$)

$$F_l^{cs} = \frac{M_{3,l}^{cs}}{\sum_{cs} M_{3,l}^{cs}} \tag{5.2}$$

and

$$I_{i,j}^{a,b} = \int_0^\infty \int_0^\infty d_{p_1}^a\ d_{p_2}^b\ \beta(d_{p_1}^w, d_{p_2}^w)\ n_i(d_{p_1}) n_j(d_{p_2})\ d(d_{p_1}) d(d_{p_2}). \tag{5.3}$$

Appendix 2: Statistical indicators

The following indicators are computed by the ATMOPY module of Polyphemus in order to evaluate error statistics for model-to-data comparisons. Let $(o_i)_i$ and $(c_i)_i$ be the observed and the modelled concentrations at time and location i, respectively. Let n be the number of data.

We define the following indicators:

- Root mean square error (rmse)

$$\sqrt{\frac{1}{n}\sum_{i=1}^{n}\left(c_i - o_i\right)^2}$$

- Correlation

$$\frac{\sum_{i=1}^{n}\left(c_i - \bar{c}\right)\left(o_i - \bar{o}\right)}{\sqrt{\sum_{i=1}^{n}\left(c_i - \bar{c}\right)^2}\sqrt{\sum_{i=1}^{n}\left(o_i - \bar{o}\right)^2}}$$

with: $\bar{o} = \frac{1}{n}\sum_{i=1}^{n} o_i$ and $\bar{c} = \frac{1}{n}\sum_{i=1}^{n} c_i$

- Mean normalised gross bias (mngb)

$$\frac{1}{n}\sum_{i=1}^{n}\frac{c_i - o_i}{o_i}$$

- Mean normalised gross error (mnge)

$$\frac{1}{n}\sum_{i=1}^{n}\frac{\left|c_i - o_i\right|}{o_i}$$

- Mean Fractionalized Bias Error (mfbe) or Mean Fractionalized Bias (mfb)

$$\frac{1}{n}\sum_{i=1}^{n}\frac{c_i - o_i}{\left(c_i + o_i\right)/2}$$

- Fractional Gross Error (fge) or Mean Fractionalized Error (mfe)

$$\frac{1}{n}\sum_{i=1}^{n}\frac{\left|c_i - o_i\right|}{\left(c_i + o_i\right)/2}$$

- Normalised Mean Bias (nmb)

$$\frac{\sum_{i=1}^{n} c_i - o_i}{\sum_{i=1}^{n} o_i}$$

- Normalised Mean Error (nme)

$$\frac{\sum_{i=1}^{n} |c_i - o_i|}{\sum_{i=1}^{n} o_i}$$

- FB

$$2\frac{\sum_{i=1}^{n} (c_i - o_i)}{\sum_{i=1}^{n} (c_i + o_i)}$$

Bibliography

Abdul-Razzak, H. et Ghan, S. (2002). A parameterization of aerosol activation 3. sectional representation. *J. Geophys. Res.*, 107:4026.

Albriet, A., Sartelet, K., Lacour, S., Carissimo, B. et Seigneur, C. (2010). Modelling aerosol number distributions from a vehicle exhaust with an aerosol CFD model. *Atmos. Env.*, 44(8): 1126–1136.

Allen, A., Harrison, R. et J.-W., E. (1989). Field measurements of the dissociation of ammonium nitrate and ammonium chloride aerosols. *Atmos. Env.*, 23:1591–1599.

Aumont, B., Szopa, S. et Madronich, S. (2005). Modelling the evolution of organic carbon during its gas-phase tropospheric oxidation: development of an explicit model based on a self generating approach. *Atmos. Chem. Phys.*, 5(9):2497–2517.

Binkowski, F. et Roselle, S. (2003). Models-3 community multiscale air quality (CMAQ) model aerosol component. 1. Model description. *J. Geophys. Res.*, 108:NO.D6, 4183.

Boulon, J., Sellegri, K., Katrib, Y., Wang, J., Miet, K., Langmann, B., Laj, P. et Doussin, J.-F. (2013). Sub-3 nm particles detection in a large photoreactor background: Possible implications for new particles formation studies in a smog chamber. *Aerosol Sc. and Tech.*, 47(2):153–157.

Boylan, J. et Russell, A. (2006). PM and light extinction model performance metrics, goals, and criteria for three-dimensional air quality models. *Atmos. Env.*, 40:4946–4959.

Camredon, M., Aumont, B., Lee-Taylor, J. et Madronich, S. (2007). The SOA/VOC/NOx system: an explicit modelling of secondary organic aerosol formation. *Atmos. Chem. Phys.*, 7(21):5599–5610.

Carlton, A., Turpin, B., Altieri, K., Seitzinger, S., Mathur, R., Roselle, S. et Weber, R. (2008). CMAQ model performance enhanced when in-cloud secondary organic aerosol is included: Comparisons of organic carbon predictions with measurements. *Environ. Sci. Technol.*, 42: 8798–8802.

Carmichael, G., Sakurai, T., Streets, D., Hozumi, Y., Ueda, H., Park, S., Fung, C., Han, Z., Kajino, M., Engardt, M., Bennet, C., Hayami, H., Sartelet, K., Holloway, T., Wang, Z., Kannari, A., Fu, J., Matsuda, M., Thongboonchoo, N. et Amann, M. (2008). MICS Asia Phase II: The Model Intercomparison Study for Asia Phase II, Methodology and overview of findings. *Atmos. Env.*, 42(15):p3468–3490.

Carmichael, G., Tang, Y., Kurata, G., Uno, I., Streets, D., Woo, J.-H., Huang, H., Yienger, J., Lefer, B., Shetter, R., Blake, D., Atlas, E., Fried, A., Apel, E., Eisele, F., Cantrell, C., Avery, M., Barrick, J., Sachse, G., Brune, W., Sandholm, S., Kondo, Y., Singh, H., Talbot, R., Bandy, A., Thorton, D., Clarke, A. et Heikes, B. (2003). Regional-scale chemical transport modeling in support of the analysis of observations obtained during the TRACE-P Experiment. *J. Geophys. Res.*, 108:D21.

Carter, W. (2010). Development of the SAPRC-07 chemical mechanism. *Atmos. Env.*, 44(40): 5324–5335.

Chang, L. et Park, S. (2004). Direct radiative forcing due to anthropogenic aerosols in East Asia during April 2001. *Atmos. Env.*, 38:4467–4482.

Chazette, P., Bocquet, M., Royer, P., Winiarek, V., Raut, J.-C., Labazuy, P., Gouhier, M., Lardier, M. et J.-P., C. (2012). EyjafjallajÃűkull ash concentrations derived from both Lidar and modeling. *J. Geophys. Res.*, 117(D00U14).

Chin, M., Rood, R., Lin, S.-J., Muller, J. et Thomspon, A. (2000). Atmospheric sulfur cycle in the global model GOCART: Model description and global properties. *J. Geophys. Res.*, 105:24671–24687.

Couvidat, F., Debry, É., Sartelet, K. et Seigneur, C. (2012a). A hydrophilic/hydrophobic organic (H2O) aerosol model: Development, evaluation and sensitivity analysis. *J. Geophys. Res.*, 117(D10304).

Couvidat, F., Kim, Y., Sartelet, K., Seigneur, C., Marchand, N. et Sciare, J. (2012b). Modeling secondary organic aerosol in an urban area: Application to Paris, France. *Atmos. Chem. Phys. Discuss.*, 12:23471–23511.

Couvidat, F., Sartelet, K. et Seigneur, C. (2012c). Investigating the impact of aqueous-phase chemistry and wet deposition on organic aerosol formation using a molecular modeling approach. *Env. Sc. and Tech.*, page submitted.

Couvidat, F. et Seigneur, C. (2011). Modeling secondary organic aerosol formation from isoprene under dry and humid conditions. *Atmos. Chem. Phys.*, 11:893–909.

Dahneke, B. (1983). *Simple Kinetic Theory of Brownian Diffusion in Vapors and Aerosols (in Theory of Dispersed Multiphase Flow)*. Meyer, R.E. Academic Press.

Davis, J., Bhave, P. et Foley, K. (2008). Parameterization of N2O5 reaction probabilities on the surface of particles containing ammonium, sulfate, and nitrate. *Atmos. Chem. Phys.*, 8(17):5295–5311.

Deboudt, K., Flament, P., ChoÃńl, M., Gloter, A., Sobanska, S. et Colliex, C. (2010). Mixing state of aerosols and direct observation of carbonaceous and marine coatings on African dust by individual particle analysis. *J. Geophys. Res.*, 115:D24207.

Debry, É., Fahey, K., Sartelet, K., Sportisse, B. et Tombette, M. (2007). Technical Note: A new SIze REsolved Aerosol Model (SIREAM). *Atmos. Chem. Phys.*, 7(6):1537–1547.

Debry, É. et Sportisse, B. (2006). Reduction of the condensation/evaporation dynamics for atmospheric aerosols: Theoretical and numerical investigation of hybrid methods. *J. Aerosol Sci.*, 37(8):950–966.

Debry, É. et Sportisse, B. (2007). Solving aerosol coagulation with size-binning methods. *Appl. Numer. Math.*, 57:1008–1020.

Dergaoui, H., Sartelet, K., Debry, É. et Seigneur, C. (2013). Modeling coagulation of externally mixed particles: sectional approach for both size and chemical composition. *jaer*, "accepted for publication".

Devilliers, M., Debry, É., Sartelet, K. et Seigneur, C. (2013). A new algorithm to solve condensation/evaporation for ultra fine, fine and coarse particles. *J. Atmos. Sci.*, 55:116–136.

Dodge, M. C. (2000). Chemical oxidant mechanisms for air quality modeling: critical review. *Atmos. Env.*, 34:2103–2130.

Donahue, N., Epstein, S., Pandis, S. et Robinson, A. (2011). A two-dimensional volatility basis set: 1. organic-aerosol mixing thermodynamics. *Atmos. Chem. Phys.*, 11:3303–3318.

Donahue, N., Robinson, A., Stanier, C. et Pandis, S. (2006). Coupled partitioning, dilution, and chemical aging of semi-volatile organics. *Environ. Sci. Technol.*, 40:2635–2643.

Epstein, S., Riipinen, I. et Donahue, N. (2010). A semiempirical correlation between enthalpy of vaporization and saturation concentration for organic aerosol. *Env. Sc. and Tech.*, 44:743–748.

Erupe, M., Viggiano, A. et Lee, S.-H. (2011). The effect of trimethylamine on atmospheric nucleation involving H2SO4. *Atmos. Chem. Phys.*, 11:4767–4775.

Fahey, K. et Pandis, S. (2003). Size-resolved aqueous-phase chemistry in a three-dimensional chemical transport model. *J. Geophys. Res.*, 108:4690.

Finlayson-Pitts, B. J. et Pitts, Jr., J. N. (2000). *Chemistry of the upper and lower atmosphere*. Academic Press, San Diego.

Gantt, B., Meskhidze, N., Facchini, M., Rinaldi, M., Ceburnis, D. et O'Dowd, C. (2011). Wind speed dependent size-resolved parameterization for the organic mass fraction of sea spray aerosol. *Atmos. Chem. Phys.*, 11:8777–8790.

GENEMIS (1994). GENEMIS (generation and evaluation of emission data. Rapport technique, EUROTRAC. annual report 1993.

Gerber, H. (1985). Relative-humidity parameterization of the navy aerosol model (NAM). Rapport technique 8956, National Research Laboratory, Washington, D.C.

Goliff, W. S. et Stockwell, W. R. (2008). The Regional Atmospheric Chemistry Mechanism, version 2, an update. University of California, Davis. International conference on Atmospheric Chemical Mechanisms. available at: `http://airquality.ucdavis.edu/pages/events/2008/acm/Goliff.pdf`.

Guenther, A., Karl, T., Harley, P., Wiedinmyer, C., Palmer, P. et Geron, C. (2006). Estimates of global terrestrial isoprene emissions using MEGAN (Model of Emissions of Gases and Aerosols from Nature). *Atmos. Chem. Phys.*, 6:3181–3210.

Han, Z., Sakurai, T., Ueda, H., Carmichael, G., Streets, D., Hayami, H., Wang, Z., Holloway, T., Engardt, M., Hozumi, H., Park, S., Kajino, M., Sartelet, K., Fung, C., Bennet, C., Thongboonchoo, N., Tang, Y., Chang, A., Matsuda, M. et Amann, M. (2008). MICS-Asia II: Model intercomparison and evaluation of ozone and relevant species. *Atmos. Env.*, 42(15):3491–3509.

Han, Z., Ueda, H., Matsuda, K., Zhang, R., Arao, K., Kanai, Y. et Hasome, H. (2004). Model study on particle size segregation and deposition during Asian dust events in March 2002. *J. Geophys. Res.*, 19:D19205.

Hänel, G. (1976). The properties of atmospheric aerosol particles as functions of the relative humidity at thermodynamic equilibrium with the surrounding moist air. *Adv. Geophys.*, 19: 73–188.

Hayami, H., Sakurai, T., Han, Z., Ueda, H., Carmichael, G., Streets, D., Holloway, T., Wang, Z., Thongboonchoo, N., Engardt, M., Bennet, C., Fung, C., Chang, A., Park, S., Kajino, M., Sartelet, K., Matsuda, K. et Amann, M. (2008). MICS-Asia II: Model intercomparison and evaluation of particulate sulfate, nitrate and ammonium. *Atmos. Env.*, 42(15):3510–3527.

Haywood, J. et Boucher, O. (2000). Estimates of the direct and indirect radiative forcing due to tropospheric aerosols: A review. *Rev. Geophys.*, 38(4):513–543.

Healy, R., Sciare, J., Poulain, L., Kamili, K., Merkel, M., MÃijller, T., Wiedensohler, A., Eckhardt, S., Stohl, A., Sarda-EstÃÍve, R., McGillicuddy, E., O'Connor, I., Sodeau, J. et Wenger, J. (2012). Sources and mixing state of size-resolved elemental carbon particles in a European megacity: Paris. *Atmos. Chem. Phys.*, 12:1681–1700.

Holloway, T., Sakurai, T., Han, Z., Ehlers, S., Spak, S., Horowitz, L., Carmichael, G., Streets, D., Hozumi, Y., Ueda, H., Park, S., Fung, C., Kajino, M., Thongboonchoo, N., Engardt, M., Bennet, C., Hayami, H., Sartelet, K., Wang, Z., Matsuda, K. et Amann, M. (2008). MICS-Asia II: Impact of global emissions on regional air quality in Asia. *Atmos. Env.*, 42(15):3543–3561.

Hughes, L., Allen, J., Bhave, P., Kleeman, M., Cass, G., Liu, D.-Y., Fergenson, D., Morrical, B. et Prather, K. (2000). Evolution of atmospheric particles along trajectories crossing the Los Angeles basin. *Env. Sc. and Tech.*, 34(15):3058–3068.

Jacob, D. (2000). Heterogeneous chemistry and tropospheric ozone. *Atmos. Env.*, 34:2131–2159.

Jacobson, M. (1999). Studying the effects of calcium and magnesium on size-distributed nitrate and ammonium with EQUISOLV II. *Atmos. Env.*, 33(22):3635–3649.

Jacobson, M. (2002). Analysis of aerosol interactions with numerical techniques for solving coagulation, nucleation, condensation, dissolution and reversible chemistry among multiple size distributions. *J. Geophys. Res.*, 107(D19):4366.

Jacobson, M., Turco, R. et Jensen, E.J.and Toon, O. (1994). Modeling coagulation among particles of different composition and size. *Atmos. Env.*, 28:1327–1338.

Johnson, D., Utembe, S., Jenkin, M., Derwent, R., Hayman, G., Alfarra, M., Coe, H. et McFiggans, G. (2006). Simulating regional scale secondary organic aerosol formation during the TORCH 2003 campaign in the southern UK. *Atmos. Chem. Phys.*, 6:403–418.

Junker, C. et Liousse, C. (2008). A global emission inventory of carbonaceous aerosol from historic records of fossil fuel and biofuel consumption for the period 1860-1997. *Atmos. Chem. Phys.*, 8:1195–1027.

Kajino, M., Ueda, H., Satsumabayashi, H. et An, J. (2004). Impacts of the eruption of Miyake-jima Volcano on air quality over far East Asia. *J. Geophys. Res.*, 19:D21204.

Kim, Y., Couvidat, F., Sartelet, K. et Seigneur, C. (2011a). Comparison of different gas-phase mechanisms and aerosol modules for simulating particulate matter formation. *J. Air Waste Manage. Assoc*, 61:1218–1226.

Kim, Y., Sartelet, K., Raut, J. et Chazette, P. (2013). Evaluation of the WRF/urban model over Greater Paris. *Boundary-Layer Meteor.*, "in revision".

Kim, Y., Sartelet, K. et Seigneur, C. (2009). Comparison of two gas-phase chemical kinetic mechanisms of ozone formation over Europe. *J. Atmos. Chem.*, 62(2):89–119.

Kim, Y., Sartelet, K. et Seigneur, C. (2011b). Formation of secondary aerosols: impact of the gas-phase chemical mechanism. *Atmos. Chem. Phys.*, 11:583–598.

Kleeman, M. et Cass, G. (2001). A 3D eulerian source-oriented model for an externally mixed aerosol. *Env. Sc. and Tech.*, 35:4834–4848.

Kleeman, M., Cass, G. et Eldering, A. (1997). Modeling the airborne particle complex as a source-oriented external mixture. *J. Geophys. Res.*, 102(D17):21355–21372.

Kuang, C., McMurry, P., McCormick, A. et Eisele, F. (2008). Dependence of nucleation rates on sulfuric acid vapor concentration in diverse atmospheric locations. *J. Geophys. Res.*, 113(D10209).

Lee-Taylor, J., Madronich, S., Aumont, B., Baker, A., Camredon, M., Hodzic, A., Tyndall, G., Apel, E. et Zaveri, R. (2011). Explicit modeling of organic chemistry and secondary organic aerosol partitioning for Mexico City and its outflow plume. *Atmos. Chem. Phys.*, 11:13219–13241.

Lohmann, U. et Feichter, J. (2005). Global indirect aerosol effects: a review. *Atmos. Chem. Phys.*, 5:715–737.

Loosmore, G. et Cederwall, R. (2004). Precipitation scavenging of atmospheric aerosols for emergency response applications: testing an updated model with new real-time data. *Atmos. Env.*, 38:993:1003.

Lu, J. et Bowman, F. (2010). A detailed aerosol mixing state model for investigating interactions between mixing state, semivolatile partitioning, and coagulation. *acp*, 10:4033–4046.

Mallet, M., Roger, J., Despiau, S., Putaud, J. et Dubovik, O. (2004). A study of the mixing state of black carbon in urban zone. *J. Geophys. Res.*, 109:D04202.

Mallet, V., Quélo, D., Sportisse, B., Ahmed de Biasi, M., Debry, É., Korsakissok, I., Wu, L., Roustan, Y., Sartelet, K., Tombette, M. et Foudhil, H. (2007). Technical Note: The air quality modeling system Polyphemus. *Atmos. Chem. Phys.*, 7(20):5479–5487.

Mallet, V. et Sportisse, B. (2006). Uncertainty in a chemistry-transport model due to physical parameterizations and numerical approximations: an ensemble approach applied to ozone modeling. *J. Geophys. Res.*, 111:D01302.

Meng, Z., Seinfeld, J., Saxena, P. et Kim, Y. (1995). Contribution of water to particulate mass in the south coast air basin. *J. Aerosol Sci.*, 22(1):111–123.

Monahan, E., Spiel, D. et Davidson, K. (1986). A model of marine aerosol generation via whitecaps and wave disruption. *In Oceanic whitecaps*, pages 167–174. D. Reidel.

Napari, I., Noppel, M., Vehkamaki, H. et Kulmala, M. (2002). Parametrization of ternary nucleation rates for h_2so_4-nh_3-h_2o vapors. *J. Geophys. Res.*, 107:D19–4381.

Nenes, A., Pandis, S. et Pilinis, C. (1999). Continued development and testing of a new thermodynamic aerosol module for urban and regional air quality models. *Atmos. Env.*, 33(10):1553–1560.

Nieminen, T., Paasonen, P., Manninen, H., Kerminen, V.-M. et Kulmala, M. (2011). Parameterization of ion-induced nucleation rates based on ambient observations. *Atmos. Chem. Phys.*, 11:3393–3402.

Odum, J., Hoffmann, T., Bowman, F., Collins, D., Flagan, R. et Seinfeld, J. (1996). Gas/particle partitioning and secondary organic aerosol yields. *Environ. Sci. Technol.*, 30:2580–2585.

Oshima, N., Koike, M., Zhang, Y., Kondo, Y., Moteki, N., Takegawa, N. et Miyazaki, Y. (2009). Aging of black carbon in outflow from anthropogenic sources using a mixing state resolved model: Model development and evaluation. *J. Geophys. Res.*, 114:D06210.

Paasonen, P., Nieminen, T., Asmi, E., Manninen, H., PetÃd'jÃd', T., Plass-DÃijlmer, C., Flentje, H., Birmili, W., Wiedensohler, A., HÃţrrak, U., Metzger, A., Hamed, A., Laaksonen, A., Facchini, M., Kerminen, V.-M. et Kulmala, M. (2010). On the roles of sulphuric acid and low-volatility organic vapours in the initial steps of atmospheric new particle formation. *Atmos. Chem. Phys.*, 10:11223–11242.

Pandis, S. et Seinfeld, J. (1989). Sensitivity analysis of a chemical mechanism for aqueous-phase atmospheric chemistry. *J. Geophys. Res.*, 94(D1):1105–1126.

Pandis, S., Seinfeld, J. et Pilinis, C. (1990). The smog-fog-smog cycle and acid deposition. *J. Geophys. Res.*, 95:18489–18500.

Pankow, J. F. (1994). An absorption model of gas/particle partitioning of organic compounds in the atmosphere. *Atmos. Env.*, 28A:185–188.

Passant, N. (2002). Speciation of UK emissions of NMVOC. Rapport technique, AEA Technology. Tech. Rep. AEAT/ENV/0545.

Pilinis, C., Capaldo, K., A., N. et S.N., P. (2000). MADM – A New Multicomponent Aerosol Dynamics Model. *Aerosol Sc. and Tech.*, 32:482–502.

Pio, C., Legrand, M., Oliveira, T., Afonso, J., Santos, C., Caseiro, A., Fialho, P., Barata, F., , Puxbaum, H., Sanchez-Ochoa, A., Kasper-Giebl, A., GelencsÃl'r, A., Preunkert, S. et Schock, M. (2007). Climatology of aerosol composition (organic versus inorganic) at nonurban sites on a west-east transect across Europe. *J. Geophys. Res.*, 112:D23S02.

Pope, C., Thun, M., Namboodiri, M., Dockery, D., Evans, J., Speizer, F. et Heath, C. (1995). Particulate air pollution as a predictor of mortality in a prospective study of U.S. adults. *Am. J. Respir. Crit. Care Med.*, 151:669–674.

Pouliot, G., Pierce, T., Denier van der Gon, H., Schaap, M., Moran, M. et Nopmongcol, U. (2012). Comparing emission inventories and model-ready emission datasets between Europe and North America for the AQMEII project. *Atmos. Env.*, 53:4–14.

Pozzoli, L., Janssens-Maenhout, G., Diehl, T., Bey, I., Schultz, M. G., Feichter, J., Vignati, E. et Dentener, F. (2011). Re-analysis of tropospheric sulfate aerosol and ozone for the period 1980-2005 using the aerosol-chemistry-climate model ECHAM5-HAMMOZ. *Atmos. Chem. Phys.*, 11:9563–9594.

Pun, B. K. et Seigneur, C. (2007). Investigative modeling of new pathways for secondary organic aerosol formation. *Atmos. Chem. Phys.*, 7:2199–2216.

Raut, J.-C. et Chazette, P. (2007). Retrieval of aerosol complex refractive index from a synergy between lidar, sunphotometer and in situ measurements during LISAIR experiment. *Atmos. Chem. Phys.*, 7:2797–2815.

Raut, J.-C. et Chazette, P. (2009). Assessment of vertically-resolved PM_{10} from mobile lidar observations. *Atmos. Chem. Phys.*, 9:8617–8638.

Real, E. et Sartelet, K. (2011). Modeling of photolysis rates over Europe: impact on chemical gaseous species and aerosols. *Atmos. Chem. Phys.*, 11:1711–1727.

Riemer, N., West, M., Zaveri, R. et Easter, R. (2009). Simulating the evolution of soot mixing state with a particle-resolved aerosol model. *J. Geophys. Res.*, 114:D09202.

Robinson, A., Donahue, N., Shrivastava, M., Weitkamp, E., Sage, A., Grieshop, A., Lane, T., Pierce, J. et Pandis, S. (2007). Rethinking organic aerosols: Semivolatile emissions and photochemical aging. *Science*, 315:1259âĂŞ1262.

Roselle, S. et Binkowski, F. (1999). Cloud dynamics and chemistry. Rapport technique, U.S. Environmental Protection Agency. EPA/600/R-99/030 chapter 11.

Roselle, S., Schere, K. et Pleim, J. (1999). Chapter 14: Photolysis rates for CMAQ, Science Algorithms of the EPA Models-3 Community Multiscale Air Quality (CMAQ) Modeling System. Rapport technique, EPA.

Roustan, Y., Sartelet, K., Tombette, M., Debry, É. et Sportisse, B. (2010). Simulation of aerosols and gas-phase species over Europe with the Polyphemus system. Part II: Model sensitivity analysis for 2001. *Atmos. Env.*, 44(34):4219–4229.

Royer, P., Chazette, P., Sartelet, K., Zhang, Q., Beekmann, M. et Raut, J.-C. (2011). Comparison of lidar-derived PM10 with regional modeling and ground-based observations in the frame of MEGAPOLI experiment. *Atmos. Chem. Phys.*, 11:10705–10726.

Russell, A. et Dennis, R. (2000). NARSTO critical review of photochemical models and modeling. *Atmos. Env.*, 34:2,283–2,234.

Sartelet, K., Couvidat, F., Seigneur, C. et Roustan, Y. (2012). Impact of biogenic emissions on air quality over Europe and North America. *Atmos. Env.*, 53:131–141.

Sartelet, K., Debry, É., Fahey, K., Roustan, Y., Tombette, M. et Sportisse, B. (2007a). Simulation of aerosols and gas-phase species over Europe with the Polyphemus system: Part I-Model-to-data comparison for 2001. *Atmos. Env.*, 41:6116–6131.

Sartelet, K., Hayami, H., Albriet, B. et Sportisse, B. (2006). Development and preliminary validation of a modal aerosol model for tropospheric chemistry: MAM. *Aerosol Sc. and Tech.*, 40(2):118–127.

Sartelet, K., Hayami, H. et B., S. (2007b). Dominant aerosol processes during high-pollution episodes over Greater Tokyo. *J. Geophys. Res.*, 112(D14214).

Sartelet, K., Hayami, H. et Sportisse, B. (2008). MICS Asia Phase II Sensitivity to the aerosol module. *Atmos. Env.*, 42(15):p3562–3570.

Schell, B., Ackermann, I., Hass, H., Binkowski, F. et Ebel, A. (2001). Modeling the formation of secondary organic aerosol within a comprehensive air quality model system. *J. Geophys. Res.*, 106:28275–28294.

Seigneur, C. (2009). Current understanding of ultrafine Particulate Matter emitted from mobile sources. *J. Air Waste Manage. Assoc*, 59(1):3–17.

Seinfeld, J. et Pandis, S. (1998). *Atmospheric Chemistry and Physics*. Wiley-interscience.

Simpson, D., Fagerli, H., Jonson, J. E., Tsyro, S., Wind, P. et Tuovinen, J.-P. (2003). Transboundary acidification, euthrophication and ground level ozone in Europe. Part I: Unified EMEP model description. Rapport technique, EMEP.

Simpson, D., Winiwarter, W., BÃűrjesson, G., Cinderby, S., Ferreiro, A., Guenther, A., Hewitt, C., Janson, R., Khalil, M., Owen, S., Pierce, T., Puxbaum, H., Shearer, M., Skiba, U., Steinbrecher, R., Tarrason, L. et Oquist, M. (1999). Inventorying emissions from nature in Europe. *J. Geophys. Res.*, 104(D7):8113–8152.

Solazzo, E., Bianconi, R., Pirovano, G., Volk, M., Vautard, R., Appel, K., Bessagnet, B., Brandt, J., Christiansen, J., Chemel, C., Coll, I., Ferreira, J., Forkel, R., Francis, X., Grell, G., Grossi, P., Hansen, A., Miranda, A., Moran, M., Nopmongcol, U., Prank, M., Sartelet, K., Schaap, M., Silver, J., Sokhi, R., Vira, J., Werhan, J., Wolke, R., Yarwood, G., Zhang,

J., Rao, S. et Galmarini, S. (2012a). Operational model evaluation for particulate matter in Europe and North America in the context of the AQMEII project. *Atmos. Env.*, 53:75–92.

Solazzo, E., Bianconi, R., Vautard, R., Appel, K., Moran, M., Hogrefe, C., Bessagnet, B., Brandt, J., Christensen, J., Chemel, C., Coll, I., Denier van der Gon, H., Ferreira, J., Forkel, R., Francis, X., Grell, G., Grossi, P., Hansen, A., Jericevic, A., Kraljevic, L., Miranda, A., Nopmongcol, U., Pirovano, G., Prank, M., Riccio, A., Sartelet, K., Schaap, M., Silver, J., Sokhi, R., Viras, J., Werhahn, J., Wolke, R., Yarwood, G., Zhang, J., Rao, S. et Galmarini, S. (2012b). Model evaluation and ensemble modelling of surface-level ozone in Europe and North America in the context of AQMEII. *Atmos. Env.*, 53:60–74.

Sportisse, B. et Dubois, L. (2002). Numerical and theoretical investigation of a simplified model for the parameterization of below-cloud scavenging by falling raindrops. *Atmos. Env.*, 36:5719–5727.

Stockwell, W., Kirchner, F., Kuhn, M. et Seefeld, S. (1997). A new mechanism for regional atmospheric chemistry modeling. *J. Geophys. Res.*, 95(D10):16343:16367.

Strader, R., Gurciullo, C., Pandis, S., Kumar, N. et Lurmann, F. (1998). Development of gas-phase chemistry, secondary organic aerosol and aqueous-phase chemistry modules for PM modeling. Rapport technique, STI.

Streets, D., Bond, T., Carmichael, G., Fernandes, S., Fu, Q., He, D., Klimont, Z., Nelson, S., Tsai, N., Wang, M., Woo, J.-H. et Yarber, K. (2003). An inventory of gaseous and primary emissions in Asia in the year 2000. *J. Geophys. Res.*, 108(D21):8809.

Troen, I. B. et Mahrt, L. (1986). A simple model of the atmospheric boundary layer; sensitivity to surface evaporation. *Boundary-Layer Meteor.*, 37:129–148.

Vautard, R., Moran, M., Solazzo, E., Gilliam, R., Matthias, V., Bianconi, R., Chemel, C., Ferreira, J., Geyer, B., Hansen, A., Jericevic, A., Prank, M., Segers, A., Silver, J., Werhahn, J., Wolke, R., Rao, S. et Galmarini, S. (2012). Evaluation of the meteorological forcing used for the Air Quality Model Evaluation International Initiative (AQMEII) air quality simulations. *Atmos. Env.*, 53:15–37.

Vehkamaki, H., Kulmala, M. et Lehtinen, K. (2003). Modelling binary homogeneous nucleation of water-sulfuric acid vapours: Parameterizations for high temperature emissions. *Env. Sci. & Tech.*, 37:3392–3398.

Vehkamaki, H., Kulmala, M., Napari, I., Lehtinen, K., Timmreck, C., Noppel, M. et Laaksonen, A. (2002). An improved parameterization for sulfuric acid-water nucleation rates for tropospheric and stratospheric conditions. *J. Geophys. Res.*, 107(D22):4622.

Wang, Z., Xie, F., Sakurai, T., Ueda, H., Han, Z., Carmichael, G., Streets, D., Engardt, M., Holloway, T., Hayami, H., Kajino, M., Thongboonchoo, N., Bennet, C., Park, S., Fung, C., Chang, A., Sartelet, K. et Amann, M. (2008). Mics-asia ii: Model inter-comparison and evaluation of acid deposition. *Atmos. Env.*, 42(15):3528–3542.

Went, F. (1960). Blue hazes in the atmosphere. *Nature*, 187:641–643.

Wesely, M. (1989). Parameterization of surface resistance to gaseous-dry deposition in regional scale numerical models. *Atmos. Env.*, 23:1293:1304.

Wexler, A. et Clegg, S. (2002). Atmospheric aerosol models for systems including the ions H+, NH4+, Na+, SO42-, NO3-,Cl-, Br-, and H2O. *J. Geophys. Res.*, 107(D14-4207).

Wexler, A. et Seinfeld, J. (1990). The distribution of ammonium salts among a size and composition dispersed aerosol. *Atmos. Env.*, 24A:1231–1246.

Wild, O., Zhu, X. et Prather, M. (2000). Fast-j: Accurate simulation of in- and below-cloud photolysis in tropospheric chemical models. *J. Atmos. Chem.*, 37(3):245–282.

Yarwood, G., Rao, S., Yocke, M. et Whitten, G. (2005). Updates to the carbon bond chemical mechanism: CB05 Final report to the US EPA, RT-0400675. available at `http://www.camx.com/publ/pdfs/CB05_Final_Report_120805.pdf`.

Yu, S., Eder, B., Dennis, R., Chu, S.-H. et Schwartz, S. (2006). New unbiased symmetric metrics for evaluation of air quality models. *Atmos. Sci. Lett.*, 7:26–34.

Zhang, L., Brook, J. et Vet, R. (2003). A revised parameterization for gaseous dry deposition in air-quality models. *Atmos. Chem. Phys.*, 3:2067–2082.

Zhang, L., Gong, S., Padro, J. et Barrie, L. (2001). A size-segregated particle dry deposition scheme for an atmospheric aerosol module. *Atmos. Env.*, pages 549–560.

Zhang, Y., McMurry, P., Yu, F. et Jacobson, M. (2010). A comparative study of nucleation parameterizations: 1. Examination and evaluation of the formulations. *J. Geophys. Res.*, 115(D20212).